



## Open Archive Toulouse Archive Ouverte (OATAO)

OATAO is an open access repository that collects the work of Toulouse researchers and makes it freely available over the web where possible

This is an author's version published in: <http://oatao.univ-toulouse.fr/25078>


**Official URL:** <https://doi.org/10.1007/s10570-019-02273-8>

### To cite this version:

Pintiaux, Thibaud<sup>ORCID</sup> and Heuls, Maëlie<sup>ORCID</sup> and Vandebossche Maréchal, Virginie<sup>ORCID</sup> and Murphy, Timothy and Wuhler, Richard and Castignolles, Patrice and Gaborieau, Marianne and Rouilly, Antoine<sup>ORCID</sup> *Cellulose consolidation under high-pressure and high-temperature uniaxial compression*. (2019) *Cellulose*, 26 (5). 2941-2954. ISSN 0969-0239

Any correspondence concerning this service should be sent to the repository administrator: [tech-oatao@listes-diff.inp-toulouse.fr](mailto:tech-oatao@listes-diff.inp-toulouse.fr)

# Cellulose consolidation under high-pressure and high-temperature uniaxial compression

Thibaud Pintiaux · Maelie Heuls · Virginie Vandebossche · Timothy Murphy · Richard Wuhrer · Patrice Castignolles · Marianne Gaborieau  · Antoine Rouilly

**Abstract** Materials based on cellulose cannot be obtained from thermoplastic processes. Our aim is to prepare all-cellulose materials by uniaxial high pressure thermocompression of cellulose. The effect of moisture content (0.8 w/w%) and temperature (175–250 °C) was characterized through the mechanical properties (bending and tensile), morphology (scanning electron microscopy, X-ray tomography) and microstructure (viscometric degree of polymerization, Raman spectroscopy, X-ray diffraction, solid-state NMR) of the specimens. The specimens were mechanically stronger in bending than in tension. They exhibited a more porous heart, a dense but very thin skin on the faces (orthogonal to the compression axis) and thick and extremely dense sides. During thermocompression severe friction between fibers caused a decrease in molecular weight while heating

above the glass transition temperature was responsible for water migration towards the specimen heart. Most of the cohesion came from the small sides of the test samples (parallel to the compression axis) and seemed mainly related to the entanglement of amorphized cellulose at the interface between particles. Around 200 °C water accumulated and provoked delamination upon pressure release, but at higher temperatures water, in a subcritical state, may have been consumed during the hydrolysis of amorphous cellulose regions. The all-cellulose material with the best mechanical properties was obtained at 2% moisture and 250 °C. This work shows that thermocompression at high temperature with limited moisture may be viable to produce renewable, sustainable all-cellulose materials for application in biobased plastic substitutes including binderless boards.

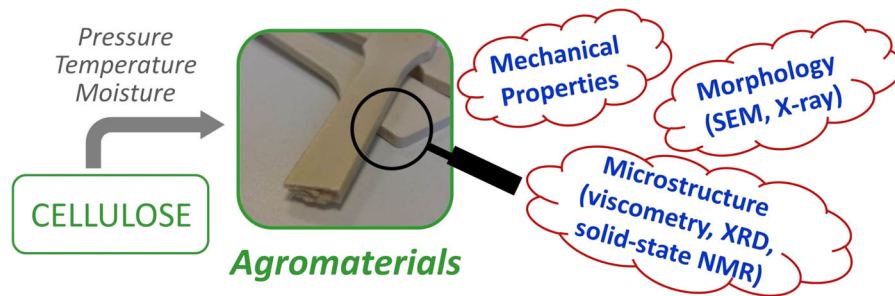
T. Pintiaux · M. Heuls · V. Vandebossche · A. Rouilly  
Laboratoire de Chimie Agro-industrielle (LCA),  
Université de Toulouse, INRA, INPT, Toulouse, France

M. Heuls · M. Gaborieau (✉)  
Medical Sciences Research Group, School of Science and  
Health, Western Sydney University, Parramatta,  
NSW 2150, Australia  
e-mail: m.gaborieau@westernsydney.edu.au

M. Heuls · P. Castignolles · M. Gaborieau  
Australian Centre for Research on Separation Science  
(ACROSS), School of Science and Health, Western  
Sydney University, Locked Bag 1797, Penrith,  
NSW 2751, Australia

T. Murphy · R. Wuhrer  
Advanced Materials Characterisation Facility (AMCF),  
Western Sydney University, Parramatta, NSW 2150,  
Australia

## Graphical abstract



**Keywords** All-cellulose materials · Compression · Mechanical properties

## Introduction

Thermoplastic processes cannot be used to produce materials from cellulose. Cellulose is a highly crystalline polymer. However, the fusion of cellulose crystallites seems only possible in very specific conditions as the energy needed to unlock the hydrogen intermolecular bonds is so high that cellulose degrades before melting. Schroeter and Felix (2005) are the only authors claiming to have achieved cellulose fusion using a combination of uniaxial compression, mechanical shear and laser beam! Most of the current forming processes for cellulose are based on dissolution/suspension in a solvent followed by drying, as for paper making. Intermolecular bonds in the native cellulose are broken by swelling and the newly formed materials gain some very interesting properties through the slow rearrangement of the chains during solvent evaporation. These materials have been called “all-cellulose composites” (Huber et al. 2012) and could also be obtained in 3D by compression in mold during drying (Obradovic et al. 2014). Additionally the current scientific rush upon nano-scaled cellulosic particles (whiskers, fibrils, crystals) has considerably increased the use of these wet processes to produce cellulose-based materials (Siró and Plackett 2010).

The most advanced dry process for cellulose is found in pharmacy: tablet compression, with microcrystalline cellulose as a common excipient (Thoorens et al. 2014). This process consists of a high-pressure, high-speed punching compression at room

temperature. The consolidation mechanism is based on porosity loss followed by particle breakage induced by the intense internal friction; it has been modelled (Michrafy et al. 2002). It produces heterogeneous materials (Busignies et al. 2006) with a slight increase in cellulose crystallinity (Kumar and Kothari 1999). To protect the active ingredient the temperature is kept low and lubricants are needed to ensure production capacity. More recently, Zhang et al. (2012) have processed cellulose with back pressure-equal channel angular pressing and obtained interesting mechanical properties. Another shearing device has been used to treat cotton linters at 180 °C and the fibers were totally destructured when processed in a dry state (Privas et al. 2013).

Our group has recently studied the uniaxial thermocompression of bio-based powders and especially of cellulose (Pintiaux et al. 2015a). This classical molding process presents the main advantage of being extremely straightforward: a very fast, dry, single step molding process. However, it had never been applied to pure cellulose, especially at high pressure (above 50 MPa). We have first shown that heating during cellulose compression triggered an additional densification of the particles bed at a specific temperature, dependent on pressure and moisture content (Jallabert et al. 2013). The particle bed densification is responsible for a marked improvement in mechanical properties of compressed cellulose. Densification seems more efficient with fiber-structured cellulose (i.e., commercial “ $\alpha$ -cellulose” vs Avicel or Vitacel), and could be related to an increase in crystallinity through co-crystallization at the interface (Vacamedina et al. 2013). This has led to a thermocompression high pressure molding process for cellulose yielding highly resistant agro-materials in very short processing durations (Pintiaux et al. 2013). The effect

of temperature is expected but difficult to predict since studying the glass transition in cellulose is challenging. Because of the hierarchical organization in cellulose fibers the dynamics of amorphous chains is hindered and most of them could be considered paracrystalline. In the 1960s and 1970s, studies of cellulose interactions with water or solvent have led to indirect measurements of a possible glass transition at extremely high temperatures: around 220–250 °C (Kargin et al. 1960; Ogiwara et al. 1970). More recently, direct thermal analyses by differential scanning calorimetry (DSC) (Szcześniak et al. 2007) and dynamic mechanical analysis (DMA) (Paes et al. 2010) have yielded more reasonable values: approximately 205 °C for dry cellulose with material pocket in DMA (Paes et al. 2010).

A threshold of 200 °C was observed in our last study (Pintiaux et al. 2013). The present work aims to investigate the best operating conditions for this kind of process, attempting in particular to increase the temperature above this threshold (up to 250 °C) and to investigate the low moisture range (0, 2, 4, 6, 8 w/w%). It also aims to better analyze the obtained materials in terms of crystallinity and chain integrity, considering especially that it is a complex material formed of at least three different domains in which cellulose properties and microstructure differ, in order to better understand the mechanism of consolidation. The crystallinity was determined both on the long range by X-ray diffraction and at the molecular level (para-crystallinity) by solid-state NMR spectroscopy.

## Materials and methods

### Materials

Cellulose was purchased from Sigma-Aldrich (St Louis, MO, USA) under the reference “ $\alpha$ -cellulose” (powder, catalog number C8002). According to the provider it exhibits 96% purity and contains 4% insoluble hemicelluloses (French et al. 2000). It was extracted from aspen trees. It is referred to as untreated cellulose in this manuscript. Bis(ethylenediamine)-copper(II) hydroxide solution (1 M in copper, molar ratio of ethylenediamine:copper of 2:1) was purchased from Sigma-Aldrich (Steinheim, Germany). It is referred to as CED solution.

### Moisture conditioning

Cellulose samples with different moisture contents were conditioned in climatic chambers (Fisher Scientific, Bioblock Scientific, Illkirch, France) set at 45% and 60% relative humidity (RH) and 25 °C producing cellulosic samples with 6.1 w/w% and 8.0 w/w% moisture content (MC), respectively. For this study, materials were equilibrated for at least 15 days. The relationship between RH and MC of cellulose samples was verified on the sorption/desorption isotherm measured at 25 °C (Jallabert et al. 2013) on a dynamic vapor sorption (DVS) apparatus (Surface Measurements System Ltd, Alperton London, UK).

Atmospheres below 30% RH are difficult to obtain in climatic chambers. To generate lower moisture contents cellulose equilibrated in standard conditions (60% RH, 25 °C, with known MC) was thus dried in a 70 °C vented oven while monitoring mass loss to reach a specific value. Dry samples were generated through drying for 48 h in an oven at 103 °C. Samples moisture contents were determined with the same drying method as above.

### Uniaxial compression

The experiments were performed in a MAPA 50 laboratory hydraulic press (Pinette Emideceau, Chalon-sur-Saône, France) in the 1A dog-bone tensile specimen as described in Pintiaux et al. (2013). Following that previous study the chosen operating conditions were: 7.5 g cellulose, 50 bar  $s^{-1}$  pressurization speed, 30 s molding time (for a total cycle time of approximately 1 min), and 300 bar maximal hydraulic pressure corresponding to a process pressure of 267 MPa. 14 dog-bone specimens were compression-molded for each of the 20 conditions (175, 200, 225, and 250 °C combined with 0, 2, 4, 6, and 8 w/w% MC). For comparison purposes, another sample was prepared in the same conditions but at 25 °C and 2 w/w% MC.

### Tensile and 3 points bending tests

Prior to testing all specimens were equilibrated for 2 weeks in the climatic chamber at 60% RH and 25 °C. Their mass was stable after about 10 days. Their mechanical properties were later observed to vary within the first 15 days but to remain

stable thereafter. Tensile and 3 point bending tests were conducted at  $1 \text{ mm min}^{-1}$  speed using a H5KT Universal testing machine (Tinius Olsen, Horsham, PA, USA) according to ISO 527-2 and ISO 178. From the stress/strain curves, the tensile modulus ( $E_t$ ), tensile strength at break ( $\sigma_t$ ), bending modulus ( $E_f$ ) and bending strength at break ( $\sigma_f$ ) were collected.

Because the compacted specimens had a heterogeneous laminar structure the tensile modulus was calculated (and not the Young's modulus). Some defects were observed on some test specimens: cracks (e.g. at  $200 \text{ }^\circ\text{C}$  and 8% MC), or lighter spots where density seemed lower resulting from an inhomogeneous mold loading. These specimens were discarded from the tests. Density was measured by buoyancy in cyclohexane as described previously (Pintiaux et al. 2013).

### X-ray tomography

A Skyscan 1174 tomograph model 1174 (Bruker, Kontich, Belgium) was used for acquisition at  $0.5^\circ$  sampling rate. Triplicates image were taken and averaged. 3-D reconstruction was performed using the Avizo software (FEI Visualization Sciences Group, Hillsboro, USA). An 8 level color scale of porosity was applied to the group of samples.

### Raman spectroscopy

Raman spectroscopy was carried on a LabRAM HR Evolution (Horiba, Kyoto, Japan). The optimal conditions with the least noise and fluorescence and significant signal intensities were: 785 nm wavelength,  $\times 100$  magnification, 100% laser power (100 mW), 5 accumulated scans, 40 s acquisition,  $1200 \text{ tr mm}^{-1}$  grating, 50 hole size,  $250 \text{ } 1500 \text{ cm}^{-1}$  Raman shift. The same global baseline was applied to all spectra which were then normalized to the most intense peak at  $1096 \text{ cm}^{-1}$ . All specimens were analyzed without sampling. Measurements were done on the sides, the faces (Fig. 1) and, after cutting them in half lengthwise, on the inner part (heart).

### Sample preparation for further analysis

To characterize the different regions of the dog-shaped specimens several grinding methods were tested using a microtome or a file. The chips obtained with the

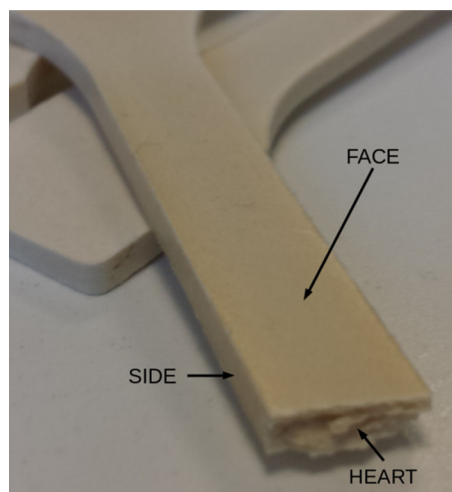


**Fig. 1** Sampling on the test specimens

microtome exhibited similar Raman spectra to that of the uncut specimens, while filed samples did not. These chips yielded higher viscometric average molecular weights than the filed samples (see Fig. S-3 in supporting information). A microtome was thus used to prepare samples (chips) for viscometry. 4 sets of operating conditions were chosen to analyze the cohesion mechanism: 8%  $25 \text{ }^\circ\text{C}$ , 0%  $175 \text{ }^\circ\text{C}$ , 2%  $250 \text{ }^\circ\text{C}$ , 8%  $175 \text{ }^\circ\text{C}$ . For each of them samples were taken from the sides, the faces and the heart (Fig. 1). Including untreated cellulose as reference 13 samples were analyzed by scanning electron microscopy (SEM), viscometry, X-ray diffraction, and solid-state NMR spectroscopy.

### Scanning electron microscopy

Electron micrographs were recorded with a LEO 435 VP (Carl Zeiss, Oberkochen, Germany) or a VEGA 3 (Tescan, Brno, Czech Republic). Before metallization all samples were dried for 24 h at  $103 \text{ }^\circ\text{C}$ .

### Viscosimetry measurements

All measurements were done in triplicate (see Table S-2) using a glass capillary-type viscometer 150 Cannon Fenske (Cannon Instrument Company, State College, PA, USA, see Fig. S-2). Each sample ( $6 \text{ g L}^{-1}$ ) was mixed with distilled water (25.0 mL) at room temperature overnight in a 50.0 mL flask. CED solution (25.0 mL) was added when the fibers seemed

totally swollen. The mixture was stirred overnight at room temperature and measured after complete dispersion. Samples 8% 175 °C sides and faces, 0% 175 °C sides and faces, 8% 25 °C sides and faces took longer to disperse (see Fig. S-4). The time for the liquid (10 mL) to pass through the viscometer bulb was used to calculate the intrinsic viscosity and determine the viscometric degree of polymerization ( $DP_v$ ) of the sample, according to the ASTM D1795-13 standard.

#### X-ray diffraction (XRD)

Crystallinity index measurements were performed on a Bruker D8 Advance Powder X-ray Diffractometer (Bruker, Melbourne, Australia) with CuK at 1.541 nm, 40 kV and 40 mA, range of  $2\theta$  from 5° to 40°, 0.02° per step, 15 s per step, Bruker Lynxseye detector, v12.0 Divergence antiscattering motorized slits, 270 mm radius goniometer. The background was determined in these conditions without sample. All X-ray diffractograms were consistent with semi-crystalline cellulose containing cellulose I crystallites (not cellulose II or III). The nomenclature recommended by French (2014) is used for Miller indices.

The crystallinity index ( $CI$ ) was determined by deconvolution (Park et al. 2010; Rebière et al. 2016). The main five crystalline peaks were fitted at 14.8°, 16.4°, 20.8°, 22.5° and 34.5°. The first four correspond to main contributions from Miller indices of (100), (010), (002), (110), and (1-10), (110), (102), (200) in cellulose  $I_\alpha$  and  $I_\beta$ , respectively. The peak at 34° contains contributions from a large number of Miller indices. For low crystallinity samples the peaks at 14.8° and 16.4° were fitted as one broad peak. The range for the amorphous phase was 15° to 22°. Topas software (Coelho Software, Brisbane, Australia) was used for the deconvolution. Gaussian functions were used. Peak positions were not reproducible on diffractograms, and the software was set to find the best position within a  $\pm 2^\circ$  range. The amorphous phase was approximatively at 21.5°, while for some authors this phase was at 18° and seemed broader (Ciolacu et al. 2011).

The crystallinity index  $CI_{XRD}$  was determined as the ratio of all crystalline peaks areas to the total area:

$$CI_{XRD} = \frac{\sum A(\text{Crystalline}) * 100}{\sum A(\text{Crystalline}) + \sum A(\text{Amorphous})}$$

where  $A(x)$  is the peak area of the peak  $x$ . For an easier comparison of the treated celluloses, not only among themselves, but also with untreated cellulose, the crystallinity indices determined by XRD were normalized with respect to that of untreated cellulose, setting the untreated cellulose crystallinity index to 100:

$$CI_{XRD,rel} = \frac{CI_{XRD}(\text{Sample}) * 100}{CI_{XRD}(\text{Untreated cellulose})}$$

The standard deviation of  $CI_{XRD}$  was estimated to be 3% by measuring 3 different parts of the heart of sample 2% 250 °C (Fig S-6). It is assumed to reflect mostly the sample heterogeneity. X-ray diffractograms are show in supporting information (Figs. S-6 to S-13).

#### Solid-state NMR spectroscopy

A Bruker Avance III 300 spectrometer (Bruker, Alexandria, Australia) operating at a  $^{13}\text{C}$  Larmor frequency of 75 MHz and a double-resonance commercial probe supporting 7 mm outer diameter MAS rotors were used. The  $^{13}\text{C}$  CP-MAS (cross polarization under magic-angle spinning) NMR spectra were recorded at 5 kHz MAS with 2 ms contact time, 1 s relaxation delay, and 5120 scans. The  $^1\text{H}$  and  $^{13}\text{C}$  pulses were calibrated with glycine. The  $^{13}\text{C}$  chemical shift scale was calibrated using the most intense cellulose signal at 76 ppm (Rebière et al. 2016).

The deconvolution of the C4 region of the  $^{13}\text{C}$  CP-MAS NMR spectrum, from 80 to 92 ppm, was carried out with the Topspin software (Bruker). It followed the approach presented by Pu et al. (2013) with crystalline signals at 89.5, 89.0, 88.8, 88.1 ppm and amorphous signals at 83.2, 84.7, 83.0 ppm (see Fig. S-23 in Appendix). The crystallinity index  $CI_{NMR}$  was determined as follows:

$$CI_{NMR} = \frac{\sum I(\text{Crystalline}) * 100}{\sum I(\text{Crystalline}) + \sum I(\text{Amorphous})}$$

where  $I(x)$  is the integral (i.e., signal area) of signal  $x$ . The  $CI_{NMR}$  is semi-quantitative, in the sense that all values are measured on the same scale, different from the actual values by the same factor. Calibrating this

scale would be lengthy and outside the scope of this study. For comparison purposes and to overcome this calibration issue the crystallinity indices determined by NMR were thus normalized with respect to that of untreated cellulose:

$$CI_{\text{NMR,rel}} = \frac{CI_{\text{NMR}}(\text{Sample}) * 100}{CI_{\text{NMR}}(\text{Untreated cellulose})}$$

Solid-state NMR spectra and their deconvolution are shown in supporting information (Figs. S-14 to S-34).

## Physical properties of molded samples

### Effect of molding temperature

Molding temperature is generally reported to be the most important parameter to improve binderless boards properties (Pintiaux et al. 2015a). However, it is also known to trigger delamination, often reported as a physical limit to the temperature increase. Delamination is a technological concern in the pharmaceutical tablets production and in the wood-based panels industry.

Surprisingly binderless boards have rarely been produced at reduced moisture content although the first results were very encouraging (Nonaka et al. 2012). Our first study (Pintiaux et al. 2013) concluded that moisture content had a limited impact on mechanical properties. The same mold as in this previous work was used. Its clearance (6  $\mu\text{m}$ ) is extremely small to avoid degassing so that moisture is trapped inside the sample during compression and delamination occurs only upon decompression. In the present work delamination was observed for about 1/3 of the specimens molded at 8% MC and 200 °C. The remaining 2/3 were tested and exhibited the best mechanical properties. The effect of temperature on mechanical properties is discontinuous: they increase with temperature until delamination is triggered. Moisture reduction below 60% RH was then expected to allow an increase in molding temperature and consequently an improvement in mechanical properties.

At 175 °C no delamination was observed for any moisture content. At 8% MC delamination was confirmed at 200 °C with about half of the specimens split in two during demolding and the other half

seeming sound but actually exhibiting a crack along the dog-bone edge. These specimens were not mechanically tested. Further increasing the temperature decreased delamination. Only some specimens exhibited slight cracks at 225 °C but none of them were truly delaminated. At 250 °C all the specimens were perfectly sound. At 0, 2 and 4% MC none of the temperatures were causing delamination. At 6% MC some specimens molded at 200 °C had slight cracks on their edge, while specimens molded at 225 and 250 °C showed no defects. It was concluded that delamination could be avoided if the conditions were kept far from 8% 200 °C.

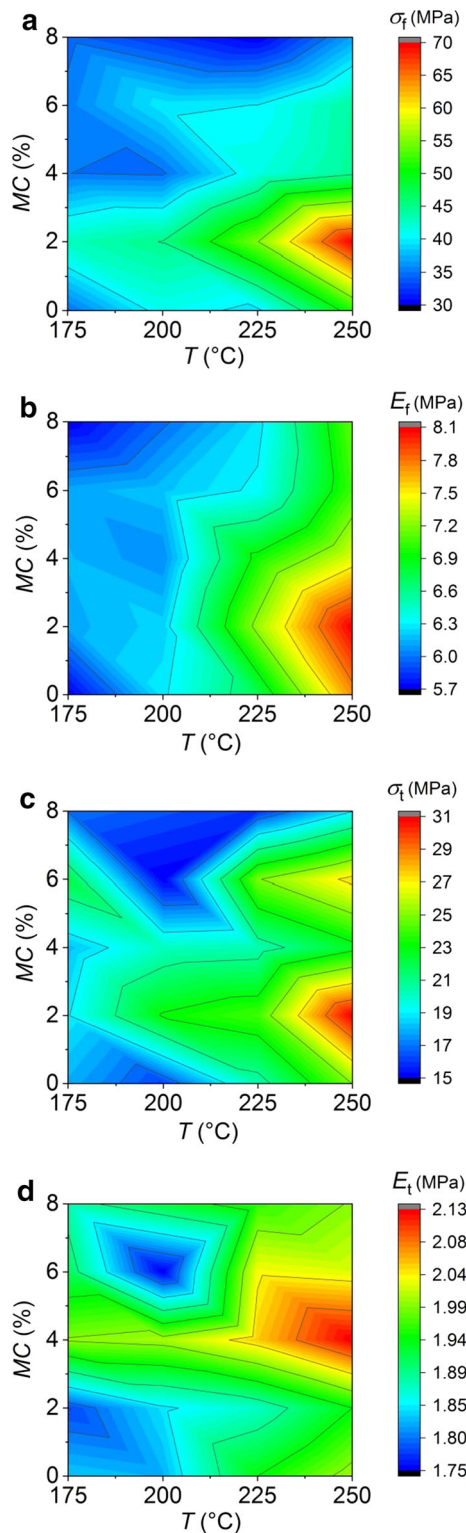
As expected higher processing temperature is also responsible for a significant improvement in water resistance of these all-cellulose materials (see Table S-1) even if they remain highly water sensitive.

### Mechanical properties

Tensile and bending tests were carried out on specimens obtained in all conditions except 8% 200 °C (Fig. 2, and Table S-3 in supporting information). At all temperatures specimens processed at 2% MC exhibited better mechanical properties than the others. Mechanical properties improved with increasing temperature at constant MC with 2 exceptions. Slight delamination resulted in the poorest mechanical properties for specimens obtained at 8% 225 °C and in the lowest tensile strength with an average bending strength for specimens obtained at 6% 200 °C.

For all operating conditions a 3 to 4 ratio was observed between the bending modulus and the tensile modulus. This highlights the heterogeneous character of the samples and particularly a marked skin effect that will be discussed later.

For specimens molded at 175 °C mechanical properties were similar over the whole moisture range except for 2% MC. For specimens molded at 200 and 225 °C the effect of moisture was limited and difficult to analyze especially for the stresses. The bending modulus had a quite smooth response; its highest value was found for 2% 250 °C and lowering temperature or increasing/decreasing moisture led to a gradual decrease in bending modulus. The tensile modulus showed a lower response to temperature variations than the other parameters.



◀ **Fig. 2** Mechanical properties of compressed cellulose according to molding temperature and cellulose moisture content; **a** bending strength at break  $\sigma_f$ , **b** bending modulus  $E_f$ , **c** tensile strength at break  $\sigma_t$ , **d** tensile modulus  $E_t$

Specimens produced at 2% 250 °C had remarkable properties and were the best specimens produced. The difference between 2% and the other moisture contents was so marked that the experiments were repeated to confirm this result. These mechanical properties reached 8.1 GPa and 31.1 MPa in bending modulus and tensile strength, respectively. These values are extremely high for materials produced through a dry process from biopolymers only (Pintiaux et al. 2015a; Rouilly and Rigal 2002). However, they are largely below the values that have been reached from wet processes especially from nano-sized cellulose (Huber et al. 2012).

The increase in mechanical properties is sharp from 200 to 250 °C. The assessment of specimens obtained at even higher temperatures would be interesting. Unfortunately these experiments could not be performed because 250 °C was the temperature limit on the laboratory press.

### Morphology of molded samples

#### A laminated structure

The commercial, untreated cellulose is composed of cellulose fibers which are hollow cylindroids of 10 to 30  $\mu\text{m}$  external diameter with a wall thickness of 3 to 5  $\mu\text{m}$ . Their length differs from one lot to another. The cellulose lot used in this work had particles with length from 100  $\mu\text{m}$  to 500  $\mu\text{m}$  and sometimes up to 1 mm (Fig. 3a).

On specimens fractured after bending tests a laminated structure was observed with sheets about 300 to 500  $\mu\text{m}$  wide aligned perpendicularly to the compression axis (Fig. 3b). Specimens broken during the tensile test also showed a layered organization but the sheets were less noticeable. In the field of intertwined materials the orthotropy resulting from the molding of fibers is classic. The same laminated structure was observed from the material breakage in the two directions of tensile and bending, it is thus inherent to the material which can be said orthotropic.



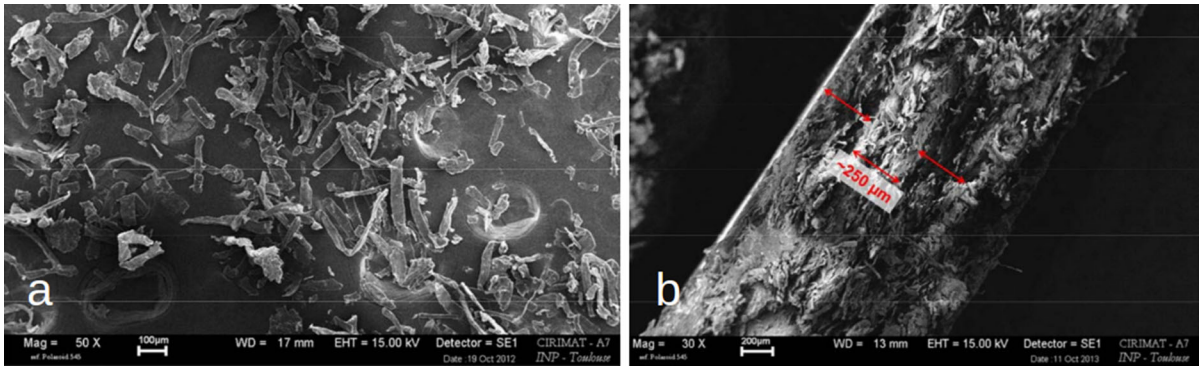


**Fig. 3** SEM micrographs of (non thermocompressed) “a cellulose”, **a** and cross section of a broken thermocompressed sample, **b** recorded on a LEO 435 VP. Scale bars are 100  $\mu\text{m}$  and 200  $\mu\text{m}$ , respectively

### A marked surface effect

For all materials produced by uniaxial compression the bending properties were stronger than the tensile properties (Fig. 2). Homogeneous materials should have stronger tensile properties than bending properties. However, the orthotropic character partially explains the opposite behavior in the case of compacted cellulose. The surface smoothness strongly differed from the core roughness of specimens. The tensile modulus of the skin was higher than that of the core while their densities were equivalent (Pintiaux et al. 2013).

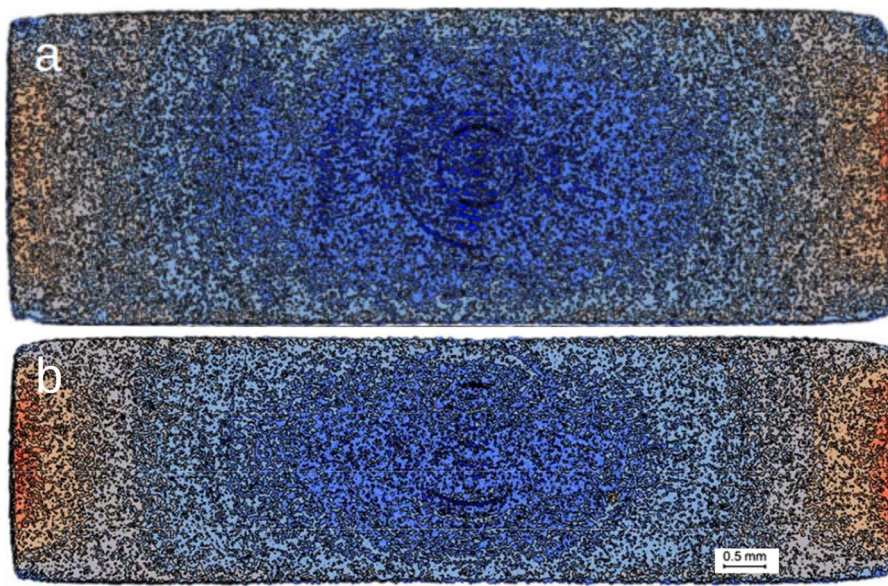
X-ray 3D tomography allowed to assess structural differences on chosen materials. After scanning the specimens on the sides a 3D image was reconstructed to visualize the porosity in the fibers direction (Fig. 4). A higher porosity was detected in the specimens core. The faces in contact with the punches (perpendicular to the pressure) were only a few  $\mu\text{m}$  thick. The surfaces in contact with the die were much thicker (about 300  $\mu\text{m}$  thick) which was surprising. On the cross section of cellulose pressed at room temperature and 8% MC (8% 25 °C) a larger zone of high porosity (deep blue) was observed in the core of the specimen (Fig. 3a). The specimen specific gravity was 1.481  $\text{g cm}^{-3}$  which was the lower than that of all other specimens. In comparison the specimen molded at 250 °C and 2% MC (2% 250 °C) had a reduced low density zone in the core and wider high density zones on the sides of the specimen (Fig. 4b). Extreme densities (red) were even observed on its lateral sides and its faces had a thicker high density area.

SEM observation revealed that on faces of this 2% 250 °C specimen (Fig. 5a) some individual fibers could still be distinguished even if in certain zones (circled in red) they seemed molten together into a continuum. At the sample core (Fig. 5b) the fibers were aggregated but were also more discernible. However, a clear brittle fracture was attempted but never obtained even with liquid nitrogen quenching, thus the observation was made from a bending test fracture and the fibers were probably pulled out during the test. The change was most obvious on the sides (Fig. 5c): no fiber could be seen and except for some cracks and bigger fractures (on the left of the figure) the surface was smooth.

### Cellulose microstructure

A previous study on different cellulose samples had shown that high pressure compression slightly increased the crystallinity rate (Vaca-Medina et al. 2013). To better understand the consolidation mechanism four samples covering a broad range of experimental conditions (8% 25 °C, 0% 175 °C, 8% 175 °C, 2% 250 °C) were thus analyzed by Raman spectroscopy. FT-IR spectroscopy on similar samples and did not reveal significant differences between samples (Pintiaux et al. 2015b); it was thus not attempted in this work. For the four chosen samples each of the main domains observed with the microtomography (i.e., heart, faces, sides) was characterized in terms of crystallinity by X-ray diffraction and solid-state NMR spectroscopy, and in terms of molecular weight by viscometry.

**Fig. 4** Sections of compressed specimens reconstructed from X ray tomography. Conditions: **a** 8% 25 °C, **b** 2% 250 °C. A color scale was applied to porosity, high porosity appeared in deep blue, medium porosity in light blue/grey, and lower porosity in orange/red. The same absolute scale was applied to both specimens



The  $DP_v$  values were lower for compacted cellulose than for untreated cellulose (Fig. 6, Table 1). The cellulose chains are thus clearly degraded during the molding process. A decrease in moisture content and an increase in temperature generally resulted in a decrease in average  $DP_v$  in all domains. The operating conditions could thus be classified from less to more degrading as follows: 8% 25 °C, 8% 175 °C, 0% 175 °C, 2% 250 °C. The maximum decrease was observed for the heart of the 2% 250 °C sample: a  $DP_v$  of 571 corresponding to a 45.2% decrease compared to untreated cellulose.

The effects of the operating conditions, especially moisture content, were different in the various sample zones. For low moisture content (0% 175 °C, 2% 250 °C) the main degradation took part in the inner sample part (heart) as if during compression the particles were too brittle to deform and were mechanically broken. For high moisture content (8% 25 °C, 8% 175 °C) the  $DP_v$  values were lowest for the faces but were very close to that of the sides. Temperature seemed to result in an overall decrease in molecular weight (Fig. 6) probably through hydrolysis and degradation reactions which were also responsible for the color changes (Fig. S-1).

Crystallinity measurements of cellulosic samples remain challenging whatever the method used (Nam et al. 2016; Park et al. 2010). To avoid degradation due to grinding Raman spectroscopy was tested first on

unbroken test samples before sampling the different domains (Fig. S-5). However, without any certitude on the orientation of the fibers spotted by the laser it seemed difficult to follow the method proposed by Agarwal et al. (2010). The samples were thus characterized by XRD and solid-state NMR spectroscopy. The crystallinity index ( $CI$ ) was determined with both techniques (Table 1) using the method giving the more meaningful results, the deconvolution (Rebière et al. 2016). The  $CI$  values determined by XRD for all heart samples were higher than those of the untreated cellulose, especially at higher moisture content at higher temperature. For the faces an opposite trend was observed,  $CI$  decreased compared to that of untreated cellulose in most cases (except for the 8% 175 °C sample) reaching 84% of that of cellulose for the 2% 250 °C sample. On the sides the  $CI$  value was always slightly higher than that of cellulose except for the 8% 25 °C sample for which a marked decrease was observed.

Solid-state NMR spectroscopy also probes the order on the molecular level. The  $CI$  values determined with solid-state NMR spectroscopy were generally lower for thermocompressed samples than for the untreated cellulose, except for the heart and faces of sample 2% 250 °C (similar values) or the heart of sample 8% 250 °C (markedly higher value). An increase in moisture content and in temperature resulted in an increase in crystallinity as measured

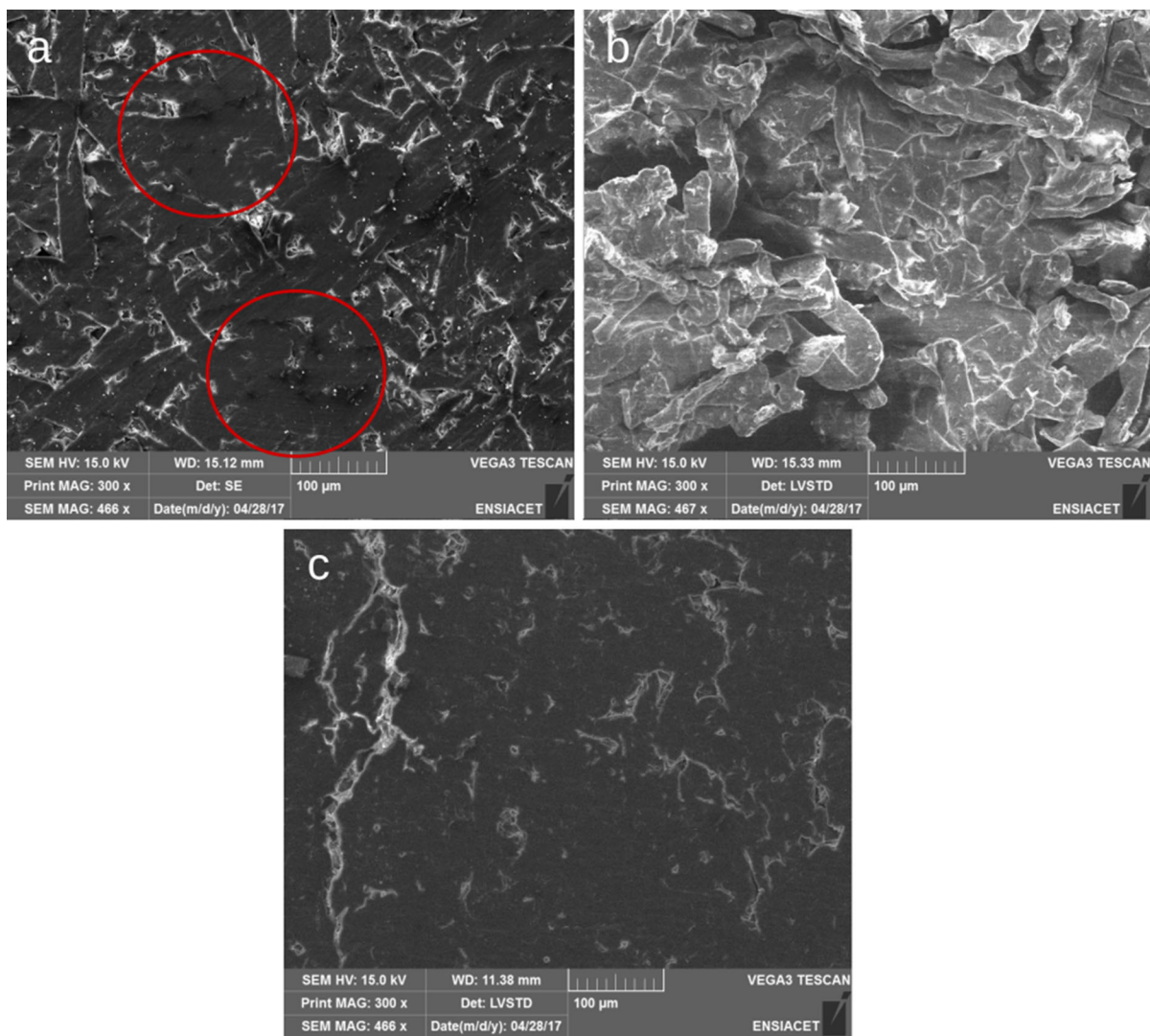


**Fig. 5** SEM micrographs of face (a), heart (b) and sides (c) of 2% 250 °C sample recorded on a VEGA 3

by solid-state NMR spectroscopy. The *CI* values determined by XRD and solid-state NMR spectroscopy were compared (Fig. S-35). No clear trend was observed. This is rationalized by taking the presence of a paracrystalline phase into account. This phase exhibits short-range ordering but lacks long-range ordering in at least one direction. Solid-state NMR spectroscopy probes molecular features at shorter length scales than X-ray diffraction (Gidley and Robinson 1990); this region will thus be interpreted as ordered (‘crystalline’) by NMR spectroscopy and as not ordered (‘amorphous’) by X-ray diffraction (Fig. S-36).

## Mechanism of cohesion

### Structural changes during compaction molding

The first step of compaction molding is the powder pre-compression which consumes most of the porosity by expelling the air between particles. This step requires very low pressure and does not produce any mechanical properties; the pre-compressed powder does not possess sufficient cohesion to be held by hand.

During the second step the particles get closer and friction occurs. This locally increases the temperature,

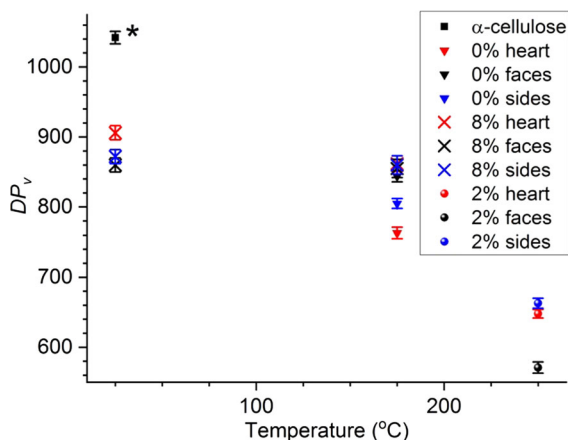


**Fig. 6** Variation of  $DP_v$  with temperature. \*This untreated cellulose was not thermocompressed and is indicated arbitrarily at 25 °C on the graph as a reference

starts the chain degradation ( $DP_v$  decreases), and further increases the density. However, the deformation of the particles is not complete as the surface area of the samples is not much affected (Vaca-Medina et al. 2013). The material resulting from cold compression (8% 25 °C) seems to be more amorphous than the original powder (Table 1) which illustrates the effect of pressure on breaking and disordering the crystallites. Cold pressed specimens consistently had an equilibrium moisture content

higher than that of the original powder which could be a result of this amorphization.

The third step consists in increasing the temperature. The temperature increase is faster and more pronounced at the material surface. During the compaction process the temperature becomes higher than a transition temperature probably related to the glass transition temperature ( $T_g$ ) of amorphous cellulose (Jallabert et al. 2013). The decrease of surface area on the resulting material compared to the original powder and to the cold-compressed material (Vaca-Medina et al. 2013) supported this hypothesis. At temperatures above the  $T_g$  the fibers can indeed be deformed; they subsequently remain in this deformed state which facilitates the establishment of the hydrogen bonding network at particles interfaces.

In the present uniaxial compression experiments the increase in temperature results in a severe improvement in mechanical properties (Table 1) which are directly impacted by the establishment of a hydrogen bonding network. An increase in density with molding temperature (Pintiaux et al. 2013) can be explained by the higher deformability of the fibers because higher temperature allowed more material (not only the surface) to reach a temperature above the  $T_g$ . The temperature increase is also responsible for a further decrease of the cellulosic chains molecular weight (Table 1). A hypothesis could thus be

**Table 1** Volumetric degree of polymerization ( $DP_v$ ) with its standard deviation in brackets, and crystallinity rate measured by XRD (deconvolution method) of the various samples tested

Sample	$DP_v$	$CI_{NMR,rel}$ (%)	$CI_{XRD}$	$CI_{XRD,rel}$ (%)	$CI_{NMR,rel}/CI_{XRD,rel}$
a cellulose	1042 (9)	100.0	50	100.0	1.00
0% 175 °C					
Heart	763 (8)	nd	50	100.0	nd
Faces	844 (8)	91.9	45	90.0	1.02
Sides	805 (7)	91.9	53	106.0	0.87
2% 250 °C					
Heart	571 (8)	100.0	52	104.0	0.96
Faces	648 (6)	100.0	42	84.0	1.19
Sides	663 (7)	89.2	53	106.0	0.84
8% 25 °C					
Heart	906 (10)	91.9	51	102.0	0.90
Faces	860 (10)	94.6	46	92.0	1.03
Sides	872 (10)	89.2	41	82.0	1.09
8% 175 °C					
Heart	862 (11)	108.1	57	114.0	0.95
Faces	855 (13)	97.3	55	110.0	0.88
Sides	860 (13)	97.3	53	106.0	0.92

Relative values are calculated in relation to the untreated cellulose value. The standard deviation of  $CI_{XRD}$  was determined on one sample to be 3 (Fig. S 6)

formulated: pressure would be responsible for the amorphization of the cellulose, and then the high temperature would allow this amorphized cellulose to reach a rubbery state and to entangle. This would occur especially in the interparticle zone where friction is the highest creating junctions and consolidating the whole specimen (Fig. 5a, c). The sintering of polymeric materials brings higher mechanical properties, lower porosity, lower BET surface area.

Surprisingly an increase in molding time did not result in a further improvement of mechanical properties (Pintiaux et al. 2013), although it should help to conduct the heat inside the material and reach a temperature above the  $T_g$  in the whole specimen.

### Role of water

Moisture was concluded to be necessary to improve mechanical properties. Jallabert et al. (2013) also confirmed that the densification step did not occur on dry cellulose from 0 to 160 °C. It is possible that the densification was not observed in this temperature range because a temperature higher than the  $T_g$  of dry cellulose (approximately 220 °C) was not reached. The mechanical properties of dry cellulose consistently strongly increased from 225 °C to 250 °C (Fig. 2).

In the present study of the concomitant effects of temperature and moisture the best mechanical properties were obtained at 2% MC which is below the monolayer of sorbed water for cellulose (5%) (Jallabert et al. 2013). Two main hypotheses can then be formulated to explain the delamination reduction at increased temperature:

- Water could be consumed in hydrolysis reactions. This would reduce the steam pressure in the inner structure during decompression. It would explain both the darkening of the specimens and the drastic decrease in cellulose molecular weight at higher temperatures in the samples core (Figs. 2, S-1). The slight increase in crystallinity measured by XRD in the heart samples would be caused by the amorphous part hydrolysis to some extent as subcritical water is known to act so (Sasaki et al. 2004). The more water and the higher the temperature, the higher  $CI$  is measured by XRD in the sample heart (Table 1).

- Water would not be consumed and steam pressure would increase but the skin strengthening due to high temperature would allow counteracting the delamination effect. This would explain why the properties are only slightly increased at 250 °C and 8% MC (Fig. 2, Table S-3) and are consistent with the cracks observed on the sample sides (Fig. 5c) because more water in the material means an increased steam pressure, and thus poorer core properties.

In most molding conditions water molecules adsorbed on cellulose are desorbed during the temperature increase and then compressed to finally reach the subcritical state. During the establishment of the hydrogen bonding network subcritical water is thus accumulated in the inner part of the material and remains there. This probably prevents the heart fibers from establishing cellulose cellulose hydrogen bonding. It could be imagined that water molecules are pushed by the pressure and temperature from the hot mold surfaces to the core of the material (because new interfibers hydrogen bonds liberate some water that may then migrate towards the heart of the sample following the temperature gradient) and that would be responsible for the apparition of the layered structure.

Upon moisture reduction high temperature is necessary to remain over the  $T_g$ , guaranteeing a strong skin capable of resisting the steam pressure inside the material. However, the moisture reduction also reduces the steam pressure and lowers the overall water quantity in the material. This gives more chances to cellulose fibers to create cohesion. Moisture is reduced and the specimens strength is increased until 2% which provides a strong skin and the least steam pressure giving maybe a higher cohesion in the core of the material. If more water is removed the thermal conductivity is lowered, and even though 250 °C is higher than the  $T_g$  the resulting skin is probably thinner or weaker as the temperature dependent cohesion mechanisms cannot take place in the inner part.

The role of water could be summarized as follows. First water reduces the  $T_g$  which is crucial for deforming particles and thus creating a hydrogen bonding network. Second it increases the thermal conductivity which permits to build up stronger cohesion at the surface and deeper at the material heart. However, without any cooling capabilities on

molds water is suddenly vaporized during the decompression and is responsible for samples delamination. This explains why the best mechanical properties are obtained at very low moisture contents.

## Conclusion

Uniaxial high pressure compression of cellulose was assessed at low moisture (0, 2, 4, 6, and 8% MC) and high temperature (175, 200, 225, and 250 °C). The best mechanical properties were obtained at 2% MC and 250 °C: modulus and maximum stress in bending of 70.1 MPa and 8.1 GPa, respectively, and modulus and maximum tensile stress of 31.1 MPa and 1.9 GPa, respectively.

The materials obtained were orthotropic showing better properties in bending than in tension. X-ray microtomography and SEM microscopy revealed a very specific morphology with a more porous heart, a dense but very thin skin on the faces (orthogonal to the compression axis) and thick and extremely dense sides where no more fibers were discernible (2%–250 °C).

During thermocompression the pressure is responsible for a harsh friction between fibers resulting in a decrease in cellulose molecular weight (as measured through the viscosity-average degree of polymerization) while temperature has a more complex role intimately related to moisture content. Heating allows reaching a temperature above the cellulose's glass transition and is responsible for the migration of water towards the sample heart. At about 200 °C it accumulates and provokes delamination when pressure is released but at higher temperatures water, in a subcritical state, may be consumed during the hydrolysis of the amorphous cellulose parts.

Most of the cohesion comes from the small sides of the test samples (parallel to the compression axis). It is mainly related to the entanglement of amorphized cellulose at the interfaces between particles.

To further improve the performance chemical modification such as esterification can be used during the pressing process (Pintiaux et al. 2015b). These findings open new perspectives for the production of 2D and 3D all-cellulose materials through a dry process.

**Acknowledgments** The French National Research Agency (ANR) and the Competitive Cluster for the Agricultural and

Food Industries in South West France (AGRIMIP) financed this study under the aegis of the HYPMOBB (High Pressure Molding of Biopolymers and Biocomposites) project. PC thanks the Academic Development Program at WSU for his stay at INP Toulouse. The authors are grateful to Brigitte Dubreuil and Manuel Marcoux for their precious help with Raman spectroscopy and X ray tomography, respectively. The authors thank the Advanced Materials Characterisation Facility (AMFC) at Western Sydney University (WSU) for the use of the X ray diffractometer and the scanning electron microscope (SEM), Matthew Van Leeuwen (WSU) for discussions on deconvolution of XRD data, as well as the School of Science and Health (WSU), and Dr James Hook, Dr Aditya Rawal (Mark Wainwright Analytical Centre, University of New South Wales) for the use of solid state NMR spectrometers. MH thanks Conseil Régional Midi Pyrénées for financial help for her stay at WSU.

## References

- Agarwal UP, Reiner RS, Ralph SA (2010) Cellulose I crystallinity determination using FT Raman spectroscopy: univariate and multivariate methods. *Cellulose* 17:721–733
- Busignies V, Leclerc B, Porion P, Evesque P, Couarraze G, Tchoreloff P (2006) Quantitative measurements of localized density variations in cylindrical tablets using X ray microtomography. *Eur J Pharm Biopharm* 64:38–50
- Ciolacu D, Ciolacu F, Popa VI (2011) Amorphous cellulose structure and characterization. *Cellul Chem Technol* 45:13–21
- French AD (2014) Idealized powder diffraction patterns for cellulose polymorphs. *Cellulose* 21:885–896
- French AD, Bertoniere NR, Brown RM, Chanzy H, Gray D, Hattori K, Glasser W (2000) Cellulose. *Kirk Othmer Encyclopedia of Chemical Technology*. Wiley, New York. <https://doi.org/10.1002/0471238961.0305121206180514.a01.pub2>
- Gidley MJ, Robinson G (1990) Techniques for studying interactions between polysaccharides, (Chapter 18). In: Dey PM, Harborne JB (eds) *Methods in Plant Biochemistry*, vol 2 Carbohydrates. Academic Press, Cambridge, pp 607–642
- Huber T, Müssig J, Curnow O, Pang S, Bickerton S, Staiger MP (2012) A critical review of all cellulose composites. *J Mater Sci* 47:1171–1186
- Jallabert B, Vaca Medina G, Cazalbou S, Rouilly A (2013) The pressure volume temperature relationship of cellulose. *Cellulose* 20:2279–2289
- Kargin PV, Kozlov VA, Van NC (1960) Classification temperature of cellulose. *Dokl Akad Nauk SSSR* 130:356–358
- Kumar V, Kothari SH (1999) Effect of compressional force on the crystallinity of directly compressible cellulose excipients. *Int J Pharm* 177:173–182
- Michrafay A, Ringenbacher D, Tchoreloff P (2002) Modelling the compaction behaviour of powders: application to pharmaceutical powders. *Powder Technol* 127:257–266
- Nam S, French AD, Condon BD, Concha M (2016) Segal crystallinity index revisited by the simulation of X ray

- diffraction patterns of cotton cellulose I $\beta$  and cellulose II. *Carbohydr Polym* 135:1–9
- Nonaka S, Umemura K, Kawai S (2012) Characterization of bagasse binderless particleboard manufactured in high temperature range. *J Wood Sci* 59:50–56
- Obradovic J, Wondraczek H, Fardim P, Lassila L, Navard P (2014) Preparation of three dimensional cellulose objects previously swollen in a DMAc/LiCl solvent system. *Cellulose* 21:4029–4038
- Ogiwara Y, Kubota H, Hayashi S, Mitomo N (1970) Temperature dependency of bound water of cellulose studied by a high resolution NMR spectrometer. *J Appl Polym Sci* 14:303–309
- Paes SS, Sun S, MacNaughtan W, Ibbett R, Ganster J, Foster TJ, Mitchell JR (2010) The glass transition and crystallization of ball milled cellulose. *Cellulose* 17:693–709
- Park S, Baker JO, Himmel ME, Parilla PA, Johnson DK (2010) Cellulose crystallinity index: measurement techniques and their impact on interpreting cellulase performance. *Biotechnol Biofuels* 3:10
- Pintiaux T, Viet D, Vandenbossche V, Rigal L, Rouilly A (2013) High pressure compression molding of alpha cellulose and effects of operating conditions. *Materials* 6:2240–2261
- Pintiaux T, Viet D, Vandenbossche V, Rigal L, Rouilly A (2015a) Binderless materials obtained by thermocompressive processing of lignocellulosic fibers: a comprehensive review. *BioResources* 10:1915–1963
- Pintiaux T, Laourine F, Vacamedina G, Rouilly A, Peydecastring J (2015b) Hydrophobic cellulose based materials obtained by uniaxial high pressure compression: in situ esterification with fatty acids and fatty anhydrides. *BioResources* 10:4626–4640
- Privas E, Felder E, Navard P (2013) Destructuration of cotton under elevated pressure. *Cellulose* 20:1001–1011
- Pu Y, Hallac B, Ragauskas AJ (2013) Plant biomass characterization: application of solution and solid state NMR spectroscopy (Chapter 18). In: Wymann CE (ed) *Aqueous pretreatment of plant biomass for biological and chemical conversion to fuels and chemicals*. Wiley, Chichester, pp 369–390. <https://doi.org/10.1002/9780470975831.ch18>
- Rebière J, Heuls M, Castignolles P, Gaborieau M, Rouilly A, Violleau F, Durrieu V (2016) Structural modifications of cellulose samples after dissolution into various solvent systems. *Anal Bioanal Chem* 408:8403–8414
- Rouilly A, Rigal L (2002) Agro materials: a bibliographic review. *J Macromol Sci Polym Rev C* 42:441–479
- Sasaki M, Adschiri T, Arai K (2004) Kinetics of cellulose conversion at 25 MPa in sub and supercritical water. *AIChE J* 50:192–202
- Schroeter J, Felix F (2005) Melting cellulose. *Cellulose* 12:159–165
- Siró I, Plackett D (2010) Microfibrillated cellulose and new nanocomposite materials: a review. *Cellulose* 17:459–494
- Szcześniak L, Rachocki A, Tritt Goc J (2007) Glass transition temperature and thermal decomposition of cellulose powder. *Cellulose* 15:445–451
- Thoorens G, Krier F, Leclercq B, Carlin B, Evrard B (2014) Microcrystalline cellulose, a direct compression binder in a quality by design environment—a review. *Int J Pharm* 473:64–72
- Vaca Medina G, Jallabert B, Viet D, Peydecastring J, Rouilly A (2013) Effect of temperature on high pressure cellulose compression. *Cellulose* 20:2311–2319
- Zhang X, Wu X, Gao D, Xia K (2012) Bulk cellulose plastic materials from processing cellulose powder using back pressure equal channel angular pressing. *Carbohydr Polym* 87:2470–2476

**Publisher's Note** Springer Nature remains neutral with regard to jurisdictional claims in published maps and institutional affiliations.

# Supplementary information for

## Cellulose consolidation under high-pressure and high-temperature uniaxial compression

Thibaud Pintiaux<sup>a</sup>, Maelie Heuls<sup>a,b,c</sup>, Virginie Vandebossche<sup>a</sup>, Timothy Murphy<sup>d</sup>, Richard Wuhrer<sup>d</sup>, Patrice Castignolles<sup>c</sup>, Marianne Gaborieau<sup>b,c,\*</sup>, Antoine Rouilly<sup>a</sup>

<sup>a</sup> *Laboratoire de Chimie Agro-industrielle (LCA), Université de Toulouse, INRA, INPT, Toulouse, France*

<sup>b</sup> *Western Sydney University, Medical Sciences Research Group, School of Science and Health, Parramatta NSW 2150, Australia*

<sup>c</sup> *Western Sydney University, Australian Centre for Research on Separation Science (ACROSS), School of Science and Health, Locked Bag 1797, Penrith, NSW 2751, Australia*

<sup>d</sup> *Western Sydney University, Advanced Materials Characterisation Facility (AMCF), Parramatta NSW 2150, Australia*

\* email: m.gaborieau@westernsydney.edu.au

### Contents

Color scale.....	S-2
Water resistance measurements .....	S-2
Viscometry .....	S-3
<i>Protocol overview</i> .....	S-3
<i>Sample preparation: chips rather than filing</i> .....	S-5
<i>Sample preparation: concentration and times</i> .....	S-6
X-ray diffraction .....	S-7
Solid-state NMR spectroscopy.....	S-12
<sup>13</sup> C CP-MAS NMR spectra.....	S-12
<i>Deconvolution of <sup>13</sup>C CP-MAS NMR spectra</i> .....	S-16
Comparison of XRD and solid-state NMR spectroscopy .....	S-21
Mechanical Properties.....	S-22
References.....	S-23



## Color scale

“ $\alpha$ -cellulose” starts to degrade around 220 to 230°C, probably because of remaining hemicelluloses. The color of the compressed specimens was then gradually darkening with temperature color (Fig. S-1). However, at a given temperature the moisture content had a lesser effect. There might be a slight correlation between lower moisture and darker. The 2 % series might also appear slightly less dark than the others, they also presented the highest mechanical properties.

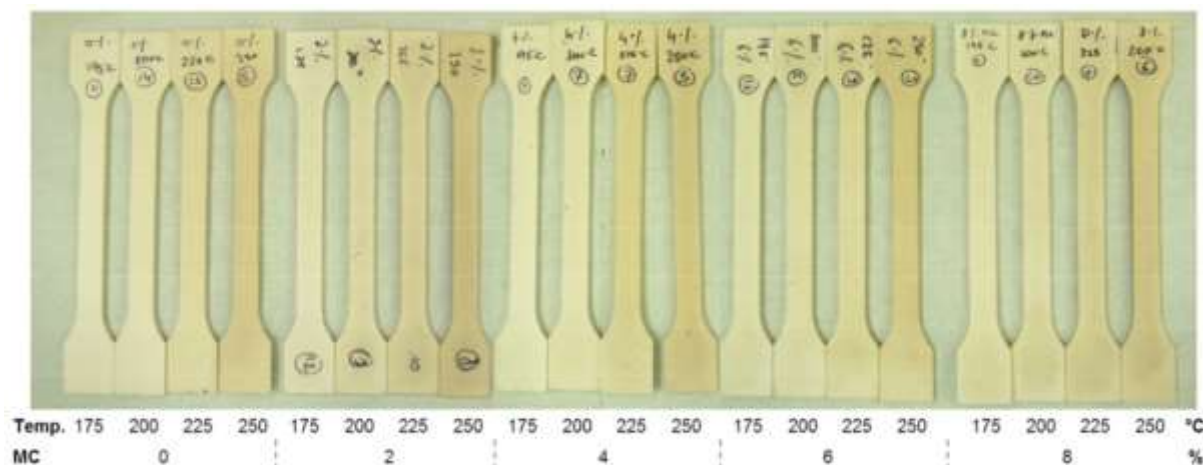


Fig. S-1: Pictures of the test specimens for the all operating conditions.

## Water resistance measurements

The water resistance was measured for 2 molding conditions (8%–175 °C, 0%–250 °C) to assess the properties of pure cellulose samples when compared to lignocellulosic materials (Table S-1). The water absorption (WA) and thickness swelling (TS) were determined. The increase in temperature from 175 °C to 250 °C resulted in a decrease of both properties by approximately 10 %. The water properties of the cellulose specimens was later seen to be better than that of any other lignocellulosic materials tested in the same conditions (work in progress) but remained low. Moisture sensitivity is clearly the main drawback of this kind of materials. An interesting fact is that they were all cracked from the middle, precisely where, if delamination had occurred, the specimen would have been opened.

Table S-1: Water absorption (WA) and thickness swelling (TS) of compressed cellulose samples. SD stands for standard deviation,

Sample	WA		TS	
	Mean	SD	Mean	SD
8%-175°C	75 %	2 %	96 %	3 %
0%-250°C	65 %	4 %	79 %	2 %

# Viscometry

## *Protocol overview*

The flow time of compacted cellulose solution in a solvent (1M Bis(ethylenediamine)copper(II) hydroxide solution, CED solution) through a capillary tube viscometer (150 mL) (Fig. S-2) at a specific concentration and temperature of 25 °C was measured.



*Fig. S-2: Capillary tube viscometer (150 mL)*

Calculations were performed using  $t_0$  (time flow of solvent without cellulose):

$$\eta_{\text{rel}} = \frac{\text{time flow of the solution}}{t_0}$$

Thanks to the table given in the standard ASTM, it was possible to estimate  $[\eta]C$  and knowing the concentration  $C$ , estimate  $[\eta]$ . Then, multiplying it by 190, it leads to the value of  $DP_v$ :

$$DP_v = 190 \cdot \frac{[\eta]C}{C}$$

$[\eta]$  = intrinsic viscosity, in  $\text{dL} \cdot \text{g}^{-1}$

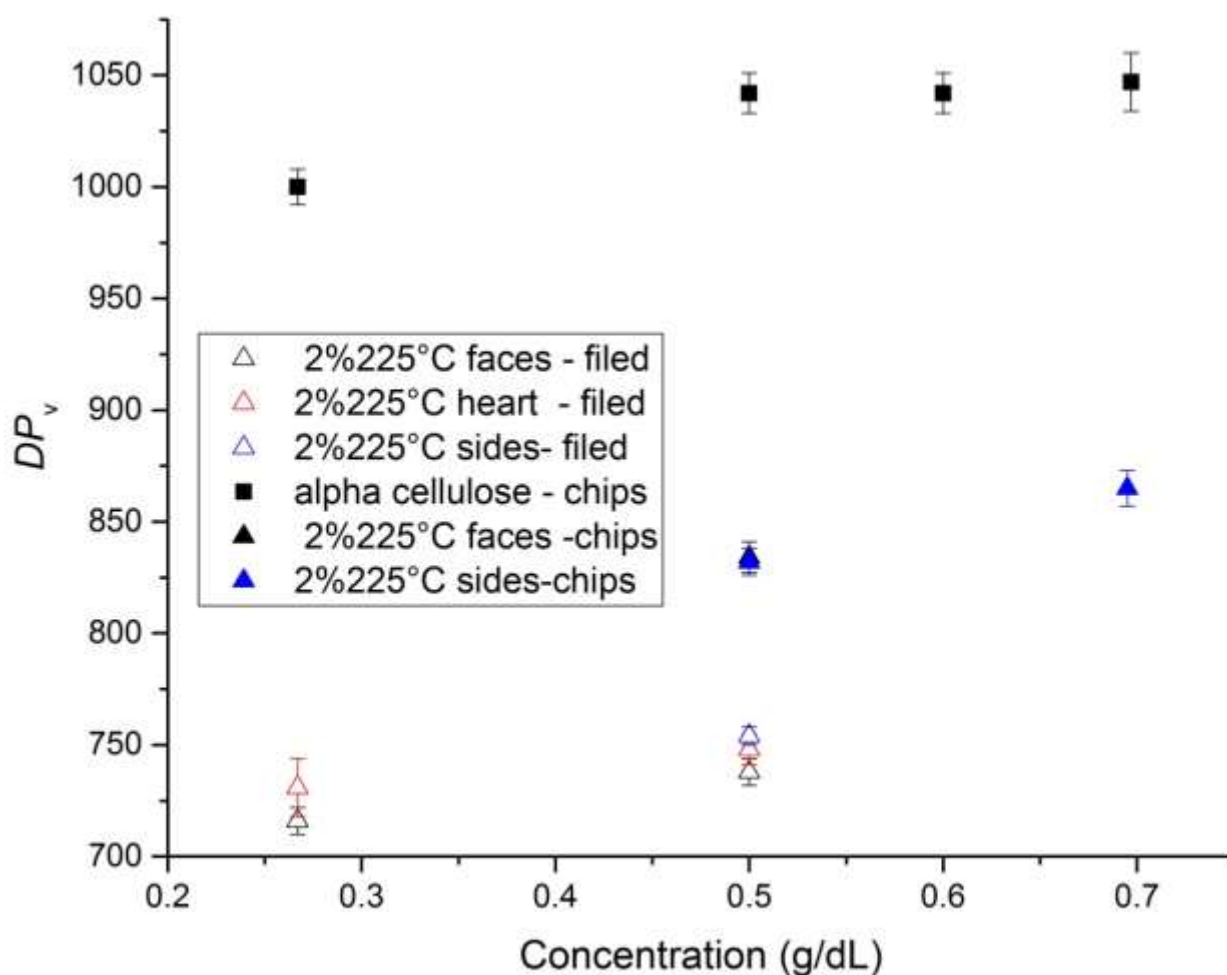
$C$  = cellulose concentration, in  $\text{g} \cdot \text{dL}^{-1}$

Table S-2 – Viscometric-average degree of polymerisation  $DP_v$  of compacted cellulose<sub>v</sub>

Sample	State	Concentration ( $g \cdot L^{-1}$ )	$DP_v$				Average $DP_v$	Standard deviation
$\alpha$ cellulose	Chips	5	1,032	1,046	1,037	1,051	1,042	9
$\alpha$ cellulose	Chips	2.67	990	1001	997	1,010	1,000	8
$\alpha$ cellulose	Chips	6	1032	1046	1037	1051	1042	9
$\alpha$ cellulose	Chips	6.97	1,036	1,052	1,036	1,063	1,047	13
0% 175°C heart	Chips	6	757	770	755	770	763	8
0% 175°C faces	Chips	6	837	852	837	851	844	8
0% 175°C sides	Chips	6	799	811	797	811	805	7
8% 25°C heart	Chips	6	901	917	893	911	906	10
8% 25°C faces	Chips	6	855	870	849	867	860	10
8% 25°C sides	Chips	6	866	881	862	880	872	10
8% 175°C heart	Chips	6	860	875	849	865	862	11
8% 175°C faces	Chips	6	858	872	840	850	855	13
8% 175°C sides	Chips	6	856	866	843	874	860	13
2% 225°C heart	Filed	2.67	736	740	736	713	731	13
2% 225°C heart	Filed	5	741	746	746	757	748	7
2% 225°C faces	Filed	2.67	708	716	716	723	716	6
2% 225°C faces	Filed	5	734	745	733	739	738	6
2% 225°C sides	Filed	5	756	755	748	756	754	4
2% 225°C faces	Chips	5	834	842	826	833	834	7
2% 225°C sides	Chips	5	833	838	823	834	832	6
2% 225°C sides	Chips	6.95	860	865	858	875	865	8
2% 250°C heart	Chips	6	564	579	564	575	571	8
2% 250°C faces	Chips	6	643	654	643	653	648	6
2% 250°C sides	Chips	6	656	667	657	670	663	7

### ***Sample preparation: chips rather than filing***

Concentrations of 5 g.L<sup>-1</sup> (250 mg in 50 mL) and 2.7 g.L<sup>-1</sup> (80 mg in 30 mL) were used for the samples of filed specimens 2%-225°C. Water (15 mL) was added to the cellulose powder in each vial with ten marbles. It was shaken for 5 h 30 min. The fibers opened and swelled. Then the CED solution previously degassed through nitrogen bubbling (15 mL) was introduced in the vial. Finally beads were added until the solution reached the edge of the vial (to avoid bubbles) and then rotated during 20 h. Using a syringe this solution (10 mL) was introduced into the viscometer and the flow time was measured in two different viscometers. For each sample four flow times were determined (Table S-2). The viscometers were conditioned by rinsing with the CED solution before each measurement. The  $DP_v$  of the specimens filed and specimens cut into chips were compared on sides and faces (5 g.L<sup>-1</sup>, 150 mg in 30 mL) and also untreated “ $\alpha$ -cellulose” (5 g.L<sup>-1</sup> and 2.7 g.L<sup>-1</sup>) (Table S-2). The  $DP_v$  values were slightly higher for compacted cellulose chips samples (Fig. S-3) compared to filed samples. Moreover, the values were not exactly the same at different concentrations (lower values at lower concentration). The samples were analyzed as chips for the rest of the work including all results presented in the main manuscript.



*Fig. S-3: Viscometric-average degree of polymerization of untreated “ $\alpha$ -cellulose” samples compressed at 2% moisture content and 225 °C, then either filed or chipped.*

### ***Sample preparation: concentration and times***

According to ASTM D1795 (January 2013) [1], the optimal conditions correspond to  $[\eta]C = 3.09 \pm 0.5 \text{ dL}\cdot\text{g}^{-1}$ . At  $C = 5 \text{ g}\cdot\text{dL}^{-1}$ ,  $[\eta]C$  values were between 1.0 and 2.80. The concentration was increased to  $7 \text{ g}\cdot\text{L}^{-1}$  (139 mg in 20 mL) to be closer to optimal conditions. The measurements were conducted with untreated “ $\alpha$ -cellulose” and compacted cellulose chips samples 2%-225°C after the following preparation: 5 h 30 min in 10 mL of water, then 20 h in 10 mL of CED solution (Table S-2). For the sides, dissolution was however incomplete (some chips were still observed in the liquid). The solutions were either too concentrated or chips must be left longer in water and/or in the CED solution. First, as the results for  $[\eta]C$  were also above 3.09, the concentration was thus fixed at  $6 \text{ g}\cdot\text{L}^{-1}$  (120 mg in 20 mL) with a longer sample preparation: 24 h in water, then 24 h in the CED solution. All compacted cellulose chips samples at 2%-225°C yielded transparent liquids (which is necessary but not sufficient for complete dissolution [2-3]). Some of the 8%-175°C and 8%-25°C samples did not yield transparent liquids (Fig. S-4) while all those 0%-175°C and 2%-225°C yielded a transparent liquid.

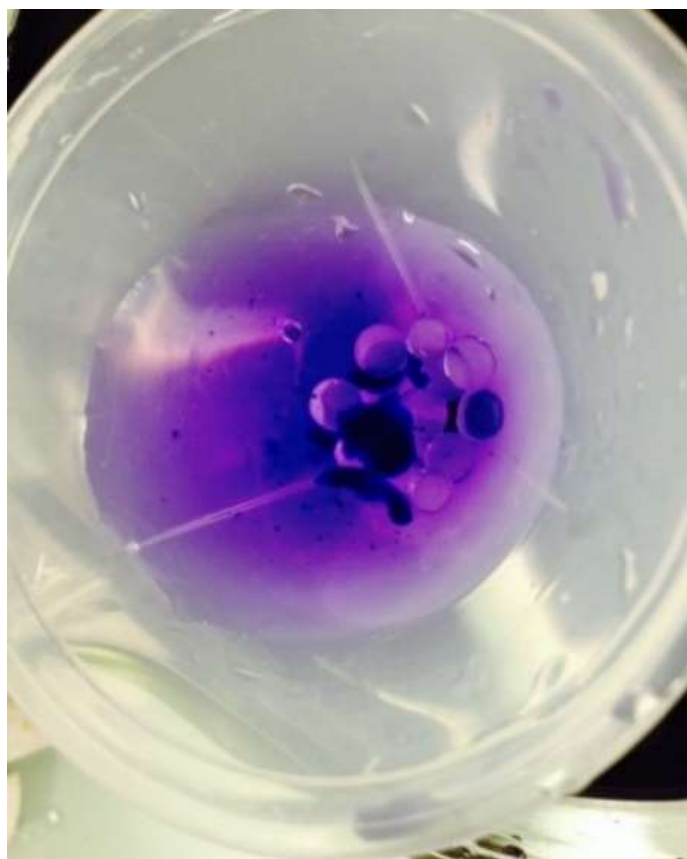


*Fig. S-4: Chips of compacted cellulose 8%-175°C faces which were not fully dissolved after treatment:  $6 \text{ g}\cdot\text{L}^{-1}$  (120 mg in 20 mL) for 24 h in 10 mL of water, 24 h in 10 mL of CED solution on a rotational shaker*

The samples that still exhibited large chips suspended after 24 h in water were left in an ultrasonic bath. Sonication did not lead to any visual change. The chips were too thick. These samples were placed on an orbital shaker. 24 h were sufficient, cellulose seemed to be opened and swollen in water. CED solution was added and the solutions were left on the shaking table during 48 h. Transparent liquids were thus obtained for these six samples: 8%-175°C sides and faces, 0%-175°C sides and faces, 8%-25°C sides and faces.

## Raman spectroscopy

To avoid degradation due to grinding Raman spectroscopy was tested first on unbroken test samples before sampling the different domains (Fig. S-5).

For all samples the Raman traces were difficult to analyze. The only significant difference was observed for the 2%-250°C specimen especially on its sides. It showed more signal in the 500  $\text{cm}^{-1}$  region and two characteristic peaks at 1260 and 1460  $\text{cm}^{-1}$  slightly less marked that are commonly attributed to amorphized cellulose [4] (Fig. S-5). However, since the sample browning is more intense on faces and sides (Fig. S-1) this behavior could also be related to the beginning of thermal degradation.

The ratio of bands intensities at 380  $\text{cm}^{-1}$  and 1096  $\text{cm}^{-1}$  should represent the crystallinity index; however, without any certitude on the orientation of the fibers spotted by the laser it seemed difficult to follow the method proposed by Agarwal et al. [5].

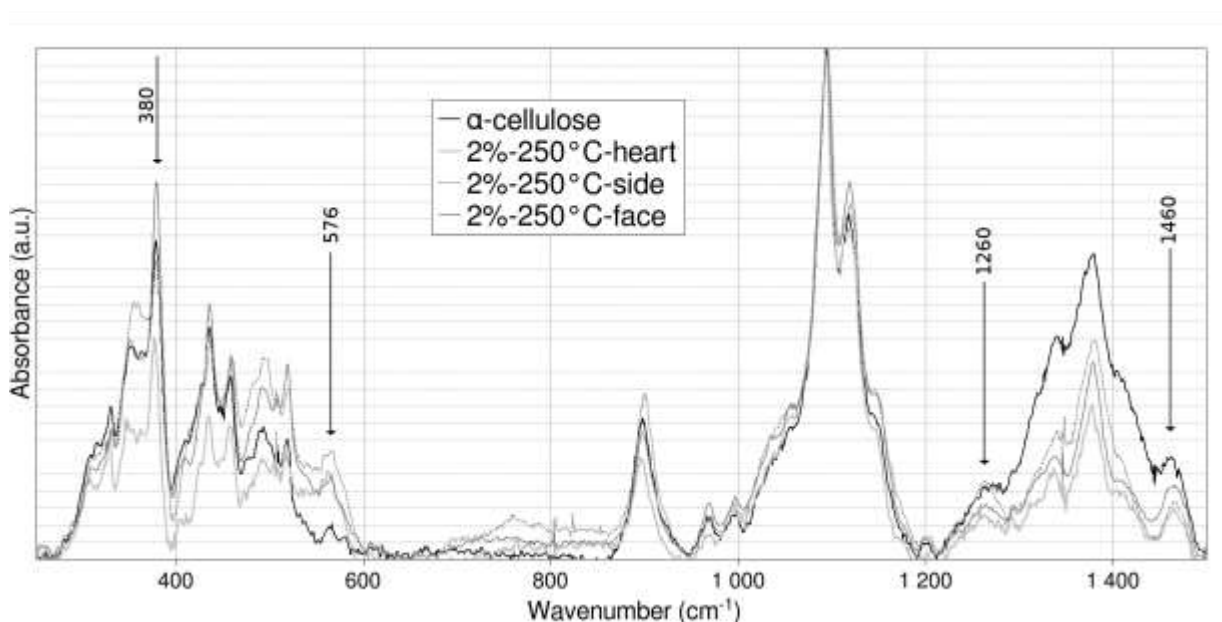


Fig. S-5: Normalized absorbance curves from Raman spectroscopy of cellulose 2%-250°C samples. The arrows indicate the wavenumbers referred to in the text.

# X-ray diffraction

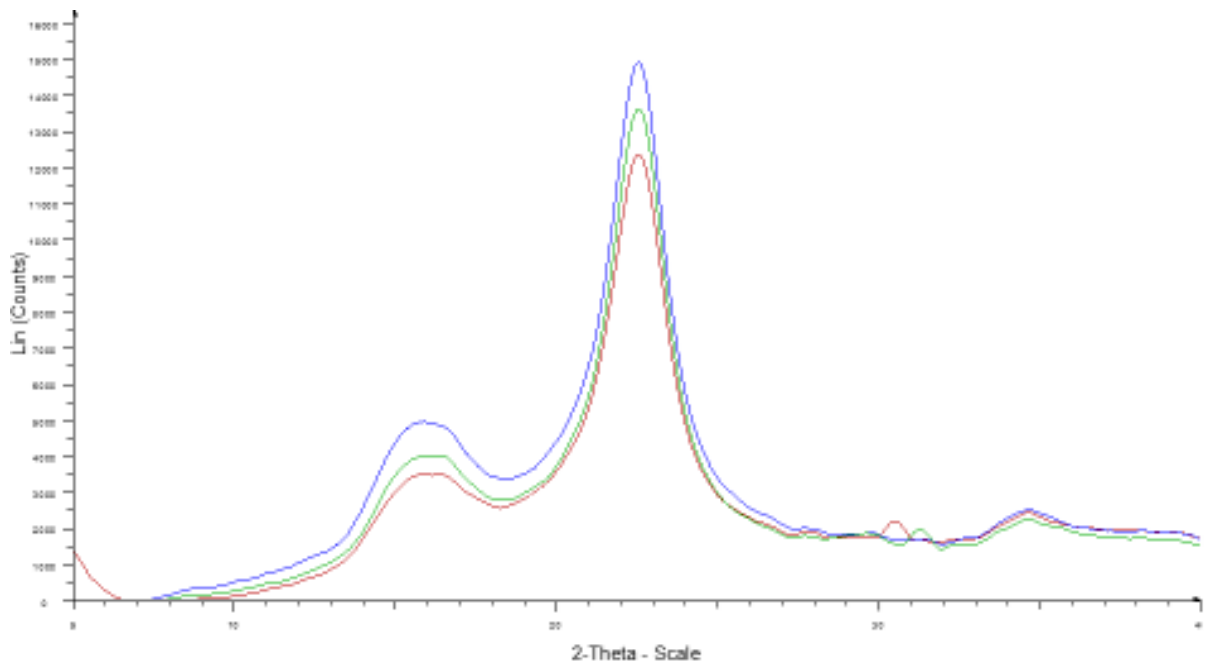


Fig. S-6: X-ray diffractograms 2%250°C heart – measure of heterogeneity – red: 2%250°C heart\_1, blue: 2%250°C heart\_2, green: 2%250°C heart\_3

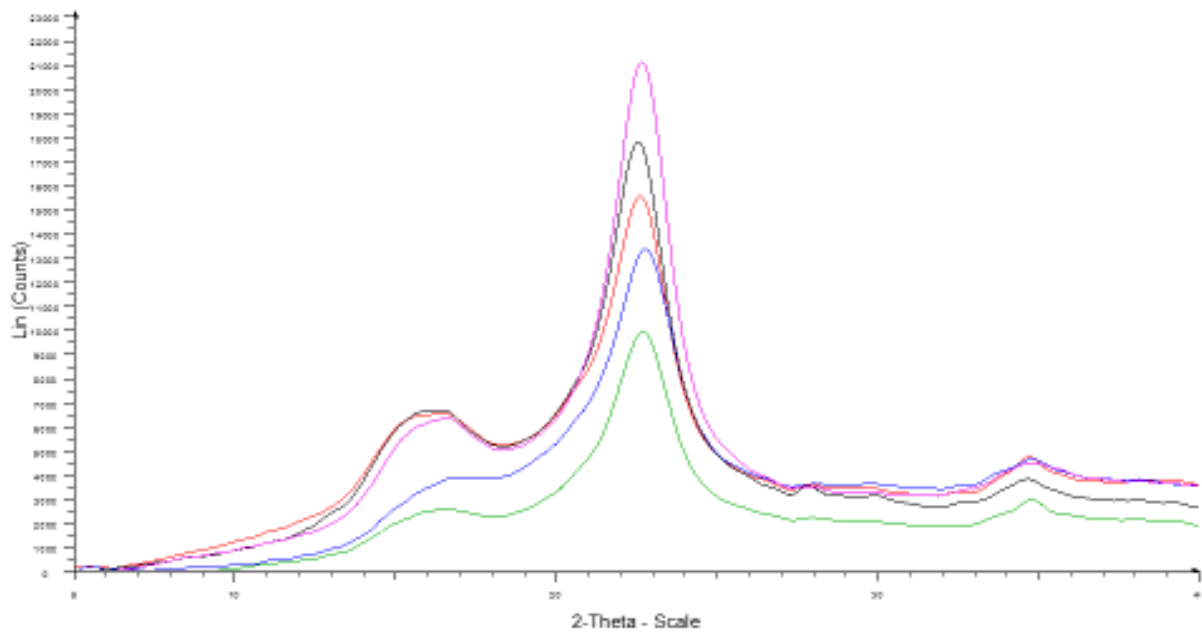


Fig. S-7: X-ray diffractograms of faces compacted cellulose – purple: 8%175°C, black: α-cellulose, red: 0%175°C, blue: 2%250°C, green: 8%25°C

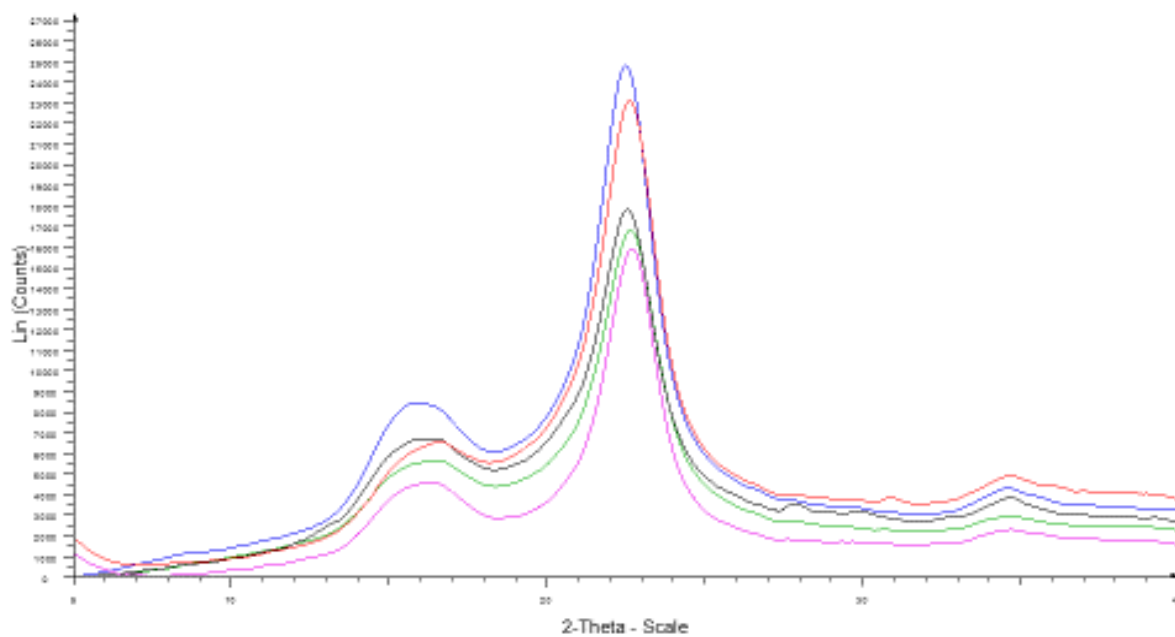


Fig. S-8: X-ray diffractograms of heart compacted cellulose – purple: 8%175°C, black: untreated “ $\alpha$ -cellulose”, red: 0%175°C, blue: 2%250°C, green: 8%25°C

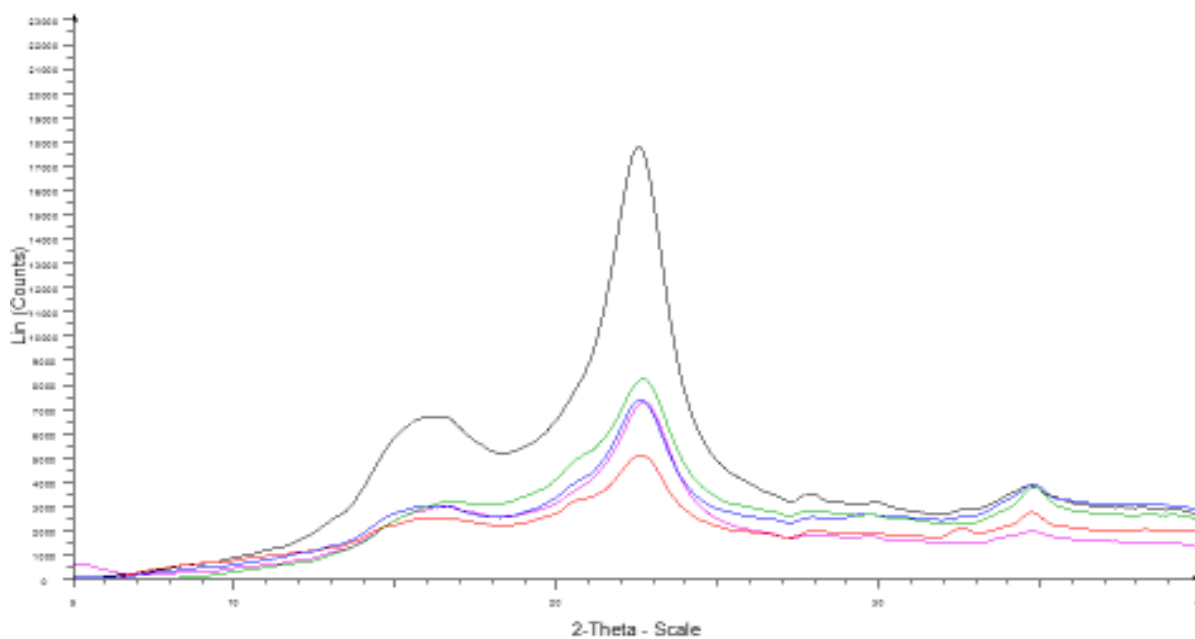


Fig. S-9: X-ray diffractograms of sides compacted cellulose – purple: 8%175°C, black: untreated “ $\alpha$ -cellulose”, red: 0%175°C, blue: 2%250°C, green: 8%25°C



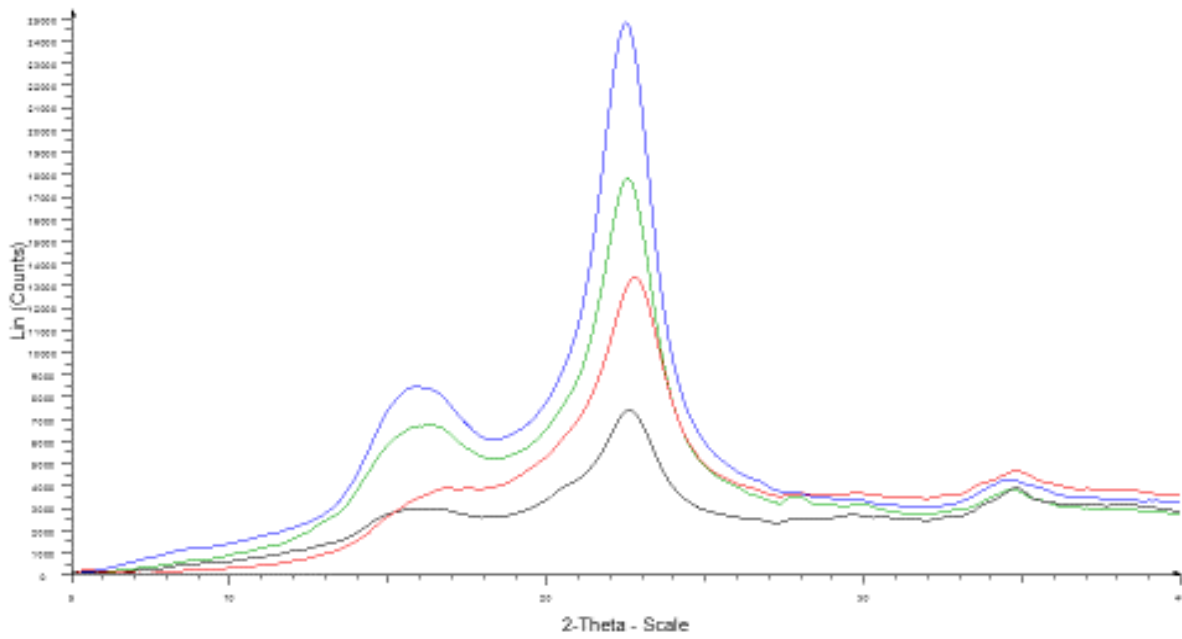


Fig. S-10: X-ray diffractograms of 2% 250°C compacted cellulose – Blue: heart, green: untreated “ $\alpha$ -cellulose”, red: faces, black: sides

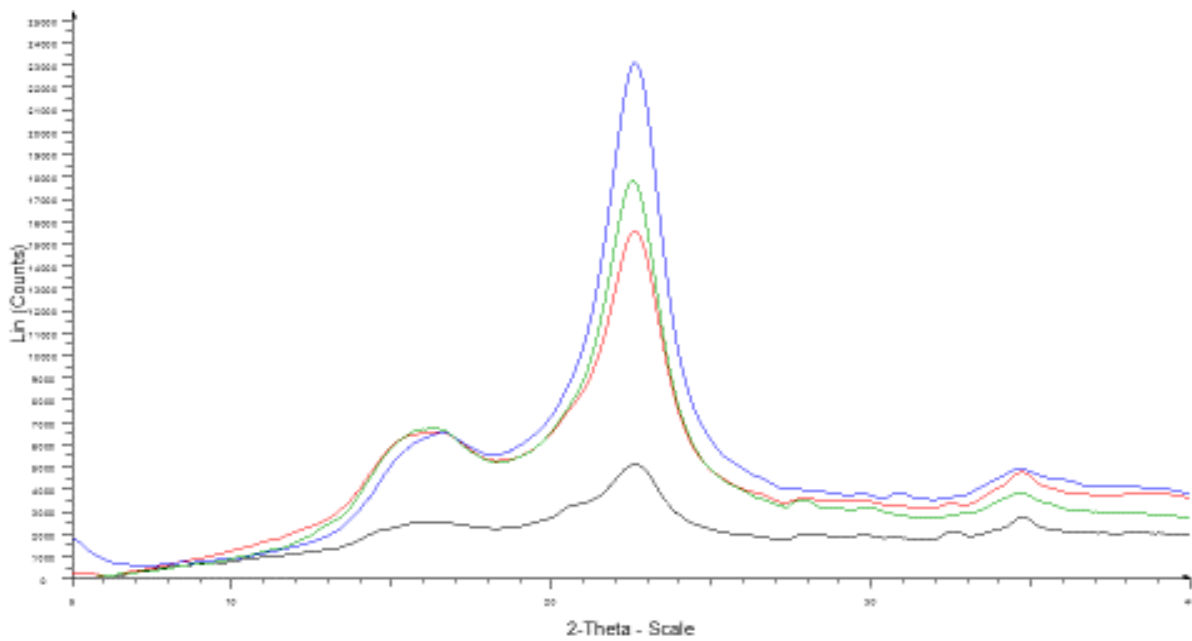


Fig. S-11: X-ray diffractograms of 0% 175°C compacted cellulose – Blue: heart, green: untreated “ $\alpha$ -cellulose”, red: faces, black: sides

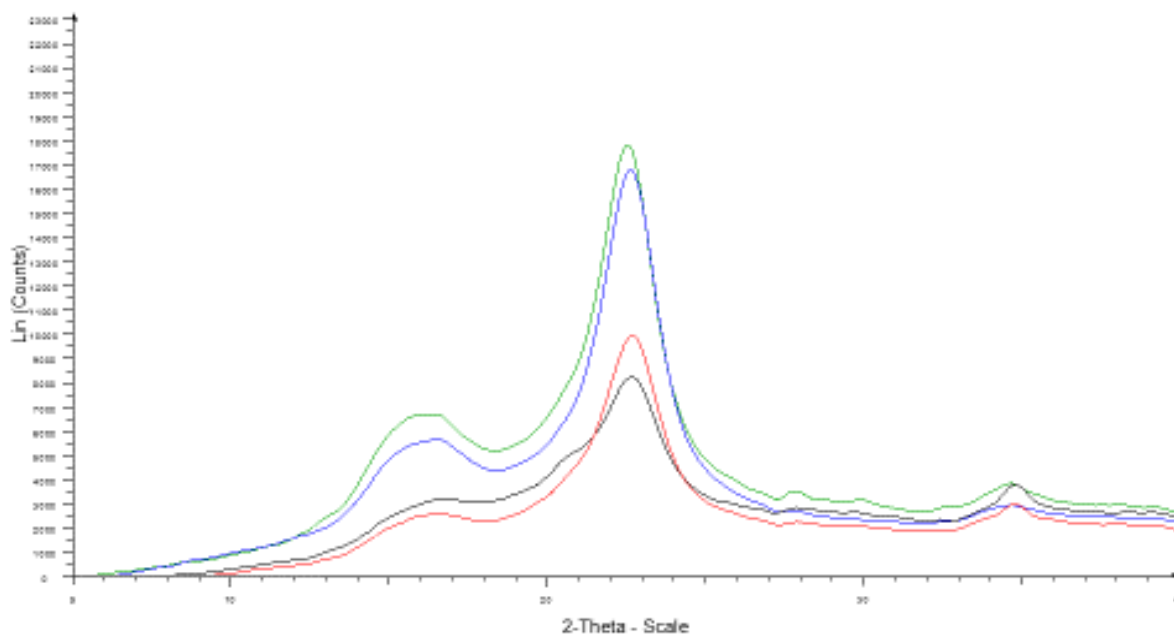


Fig. S-12: X-ray diffractograms of 8% 25°C compacted cellulose – Blue: heart, green: untreated “ $\alpha$ -cellulose”, red: faces, black: sides

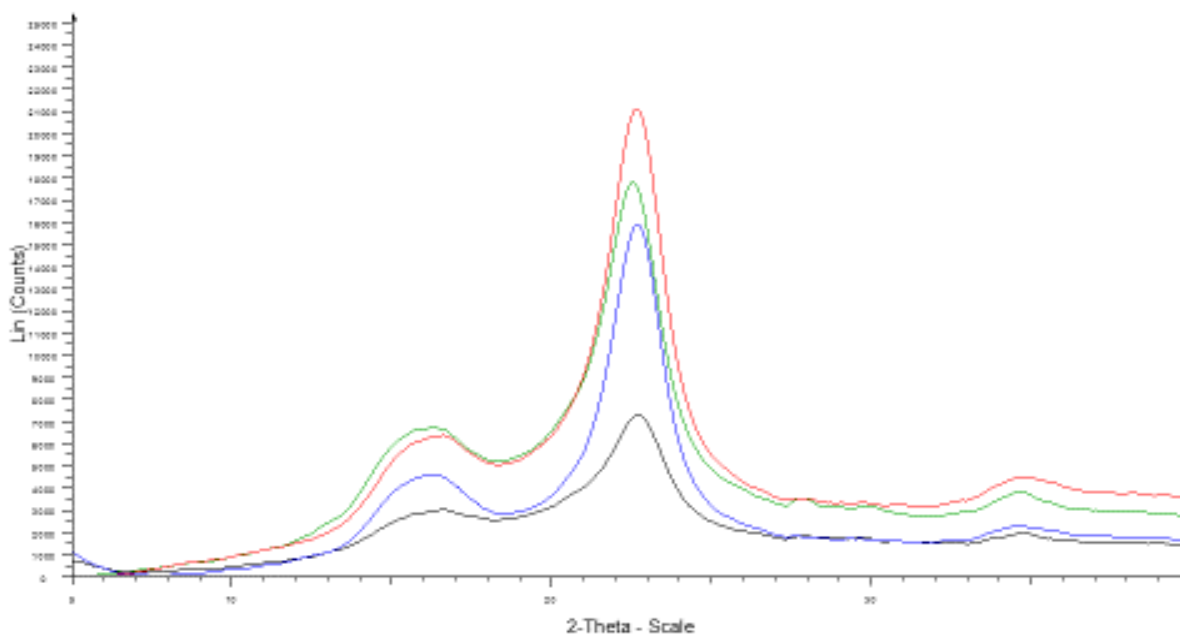


Fig. S-13: X-ray diffractograms of 8% 175°C compacted cellulose – Blue: heart, green: untreated “ $\alpha$ -cellulose”, red: faces, black: sides

# Solid-state NMR spectroscopy

## $^{13}\text{C}$ CP-MAS NMR spectra

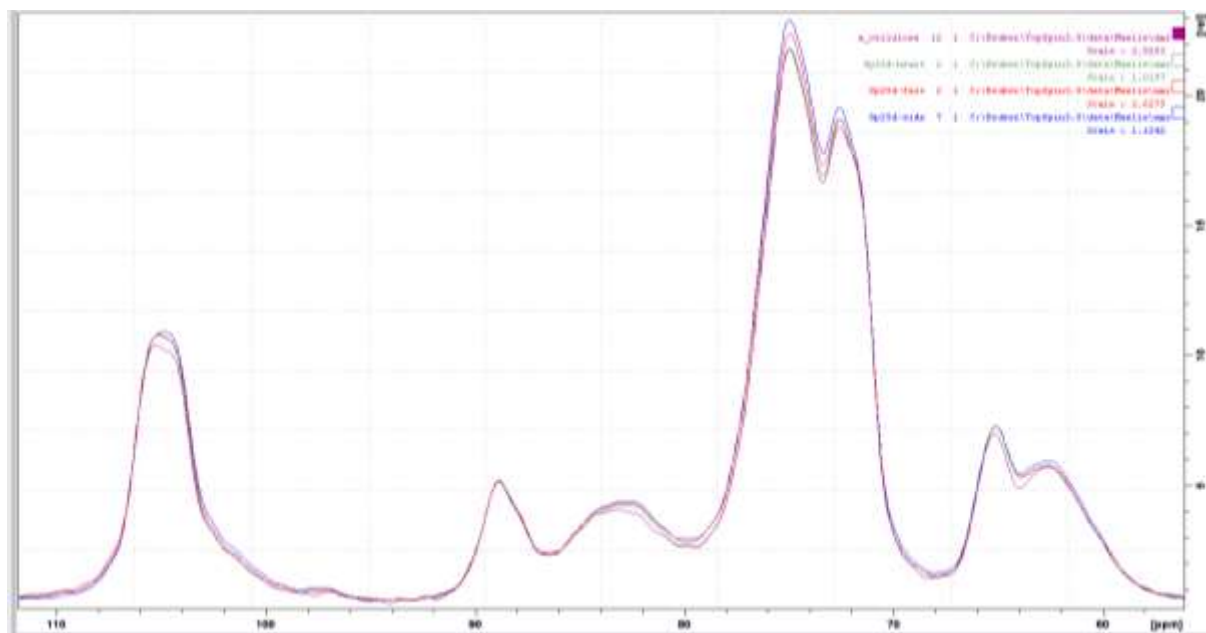


Fig. S-14: Spectra of compacted cellulose 8%25°C – full  $^{13}\text{C}$  CP-MAS NMR spectra – purple: untreated “ $\alpha$ -cellulose”, green: heart, blue: sides, red: faces

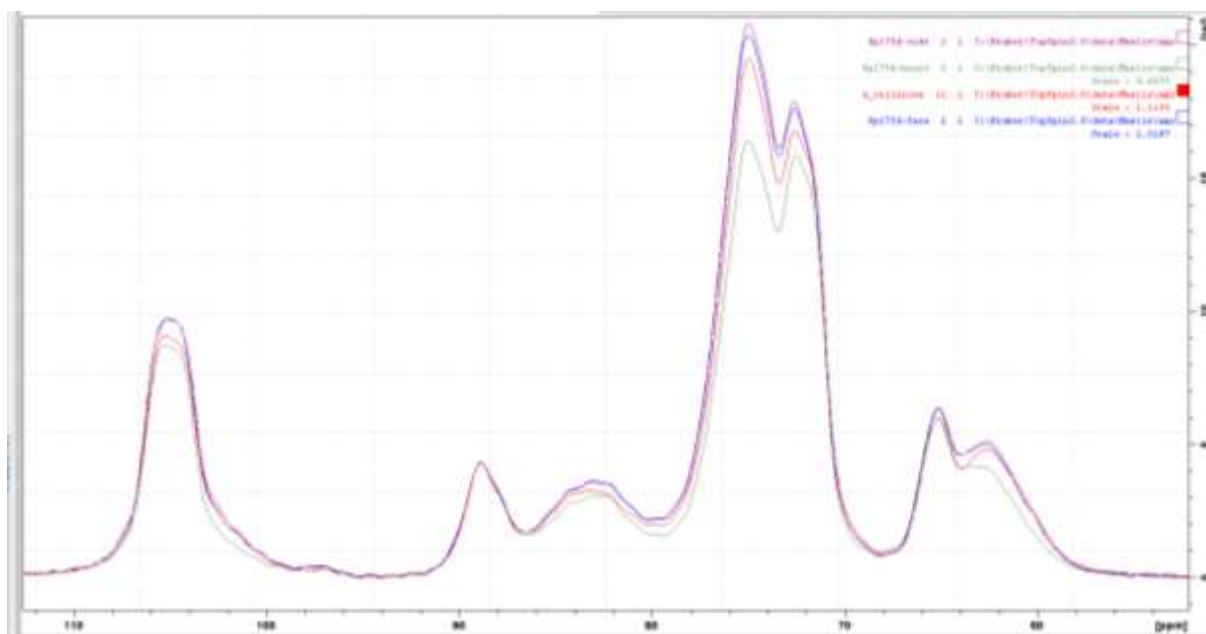


Fig. S-15: Spectra of compacted cellulose 8%175°C – full  $^{13}\text{C}$  CP-MAS NMR spectra – purple: sides, green: heart, blue: faces, red: untreated “ $\alpha$ -cellulose”

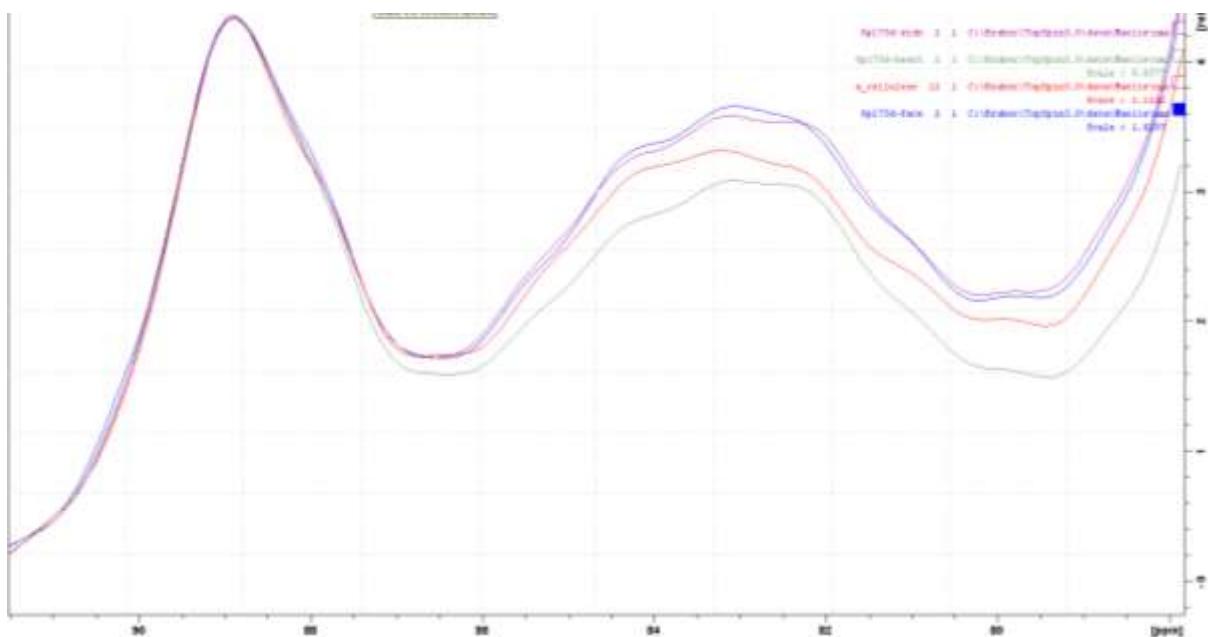


Fig. S-16: Spectra of compacted cellulose 8%175°C - the C4 region of  $^{13}\text{C}$  NMR spectra – purple: sides, green: heart, blue: faces, red: untreated “ $\alpha$ -cellulose”

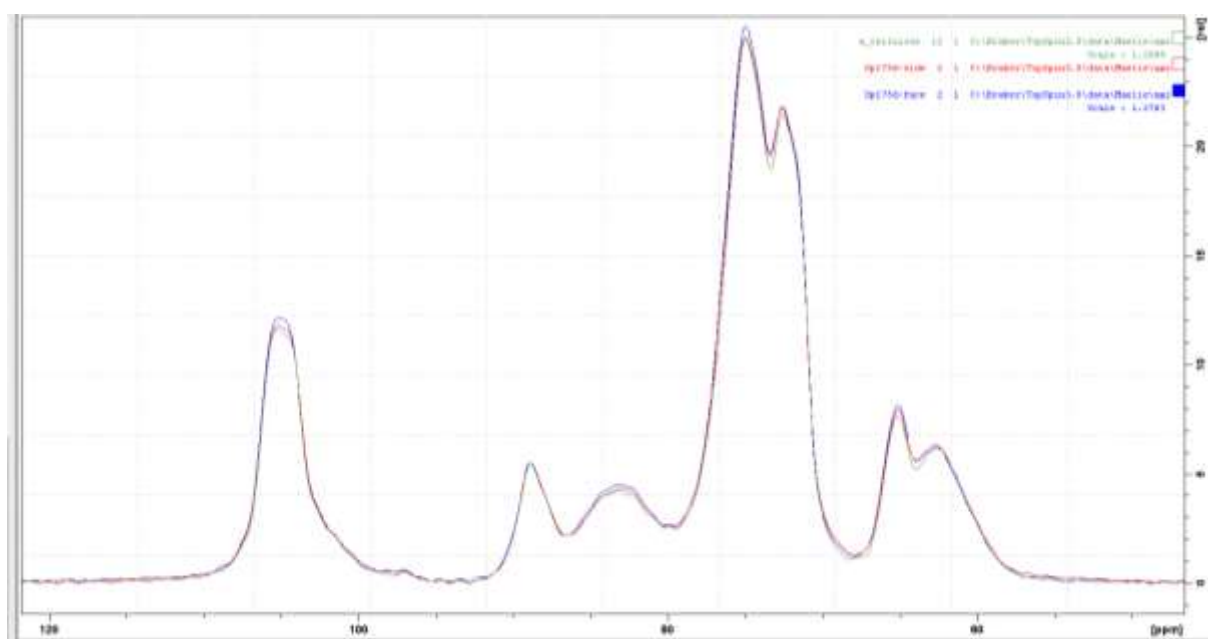


Fig. S-17: Spectra of compacted cellulose 0%175°C – full  $^{13}\text{C}$  CP-MAS NMR spectra – green: untreated “ $\alpha$ -cellulose”, blue: faces, red: sides

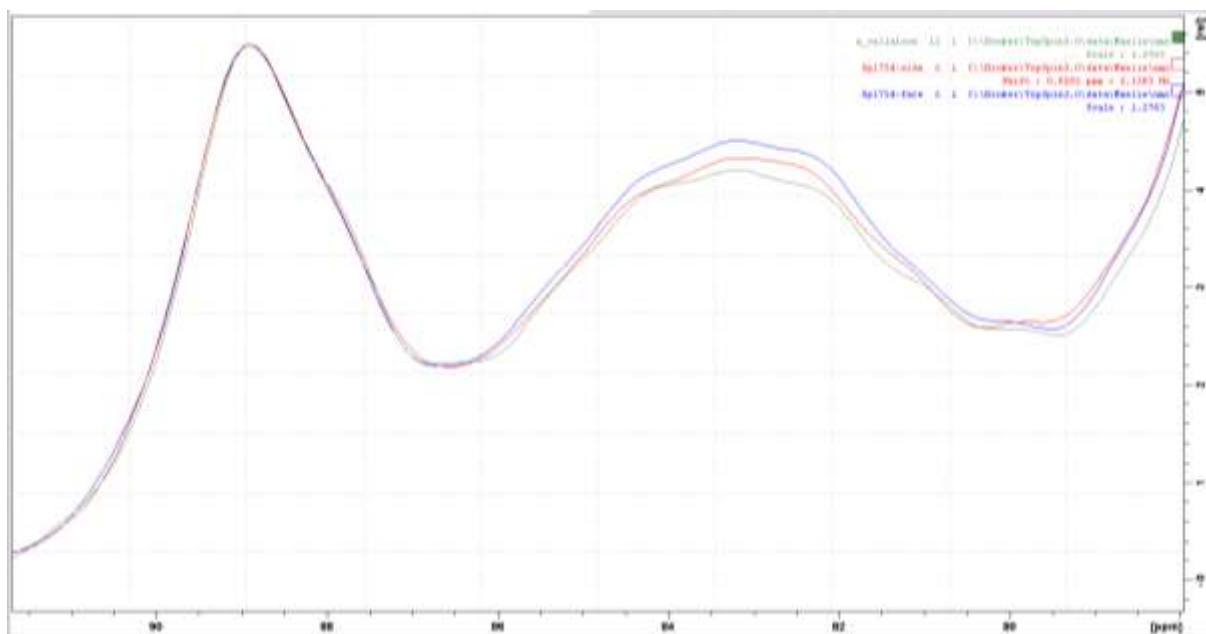


Fig. S-18: Spectra of compacted cellulose 0%175°C - the C4 region of  $^{13}\text{C}$  CP-MAS NMR spectra – green: untreated “ $\alpha$ -cellulose”, blue: faces, red: sides

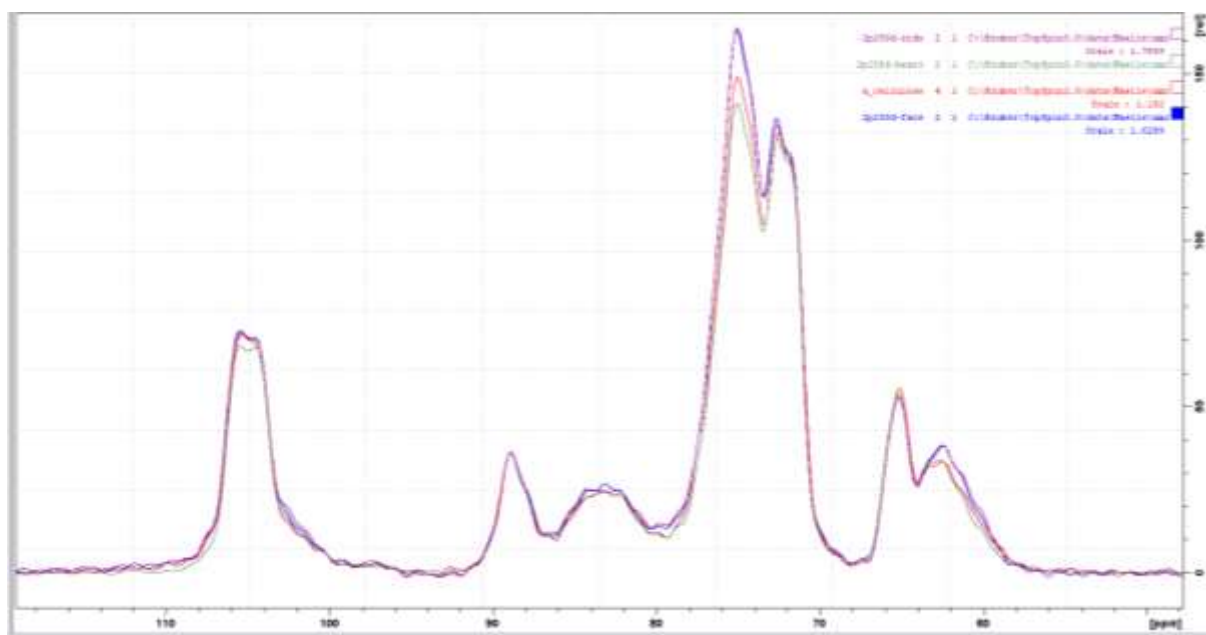


Fig. S-19: Spectra of compacted cellulose 2%250°C – full  $^{13}\text{C}$  CP-MAS NMR spectra – purple: sides, green: heart, blue: faces, red: untreated “ $\alpha$ -cellulose”

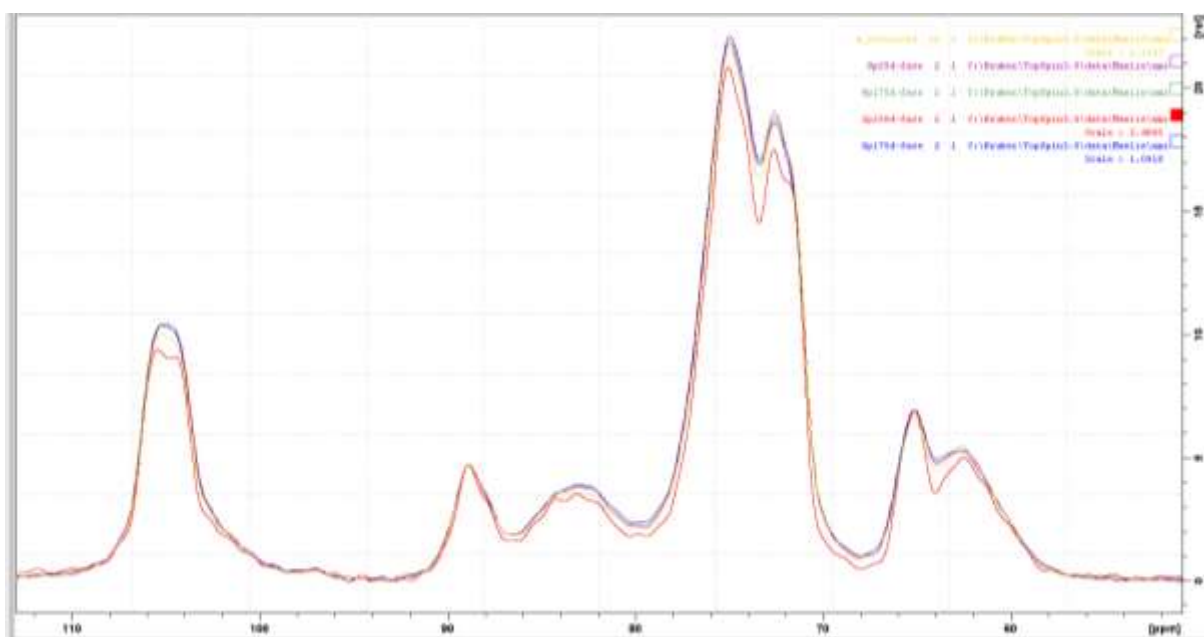


Fig. S-20: Spectra of compacted cellulose faces – full  $^{13}\text{C}$  CP-MAS NMR spectra – purple: 8%25°C, green: 8%175°C, red: 2%250°C, blue: 0%175°C, yellow: untreated “ $\alpha$ -cellulose”

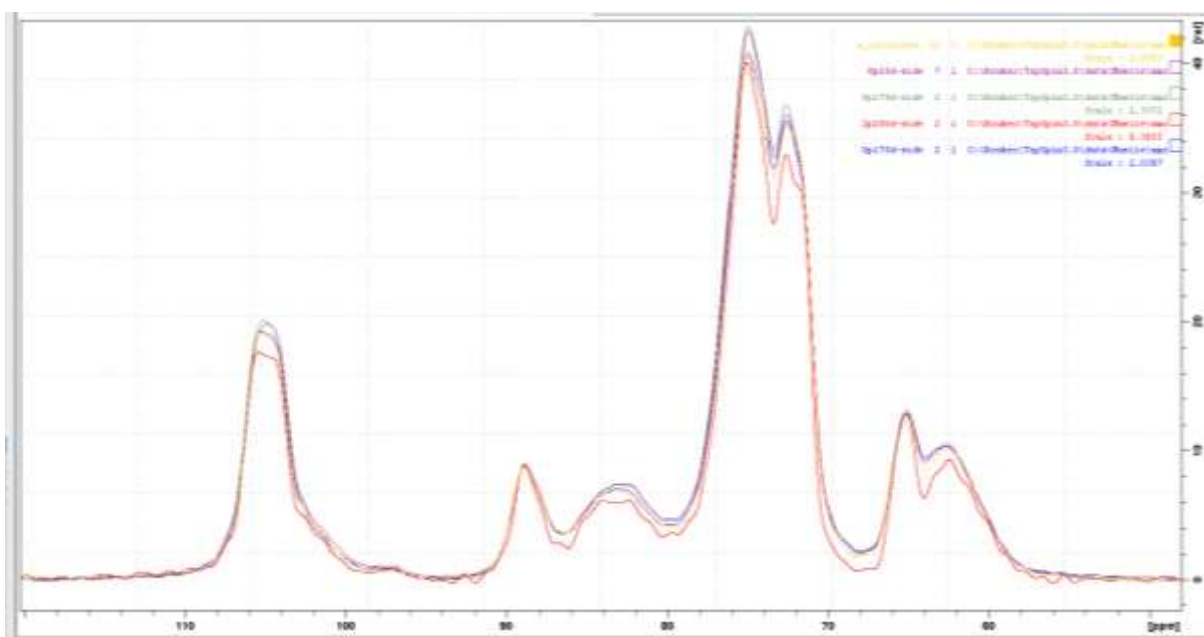


Fig. S-21: Spectra of compacted cellulose sides – full  $^{13}\text{C}$  CP-MAS NMR spectra – purple: 8%25°C, green: 8%175°C, red: 2%250°C, blue: 0%175°C, yellow: untreated “ $\alpha$ -cellulose”

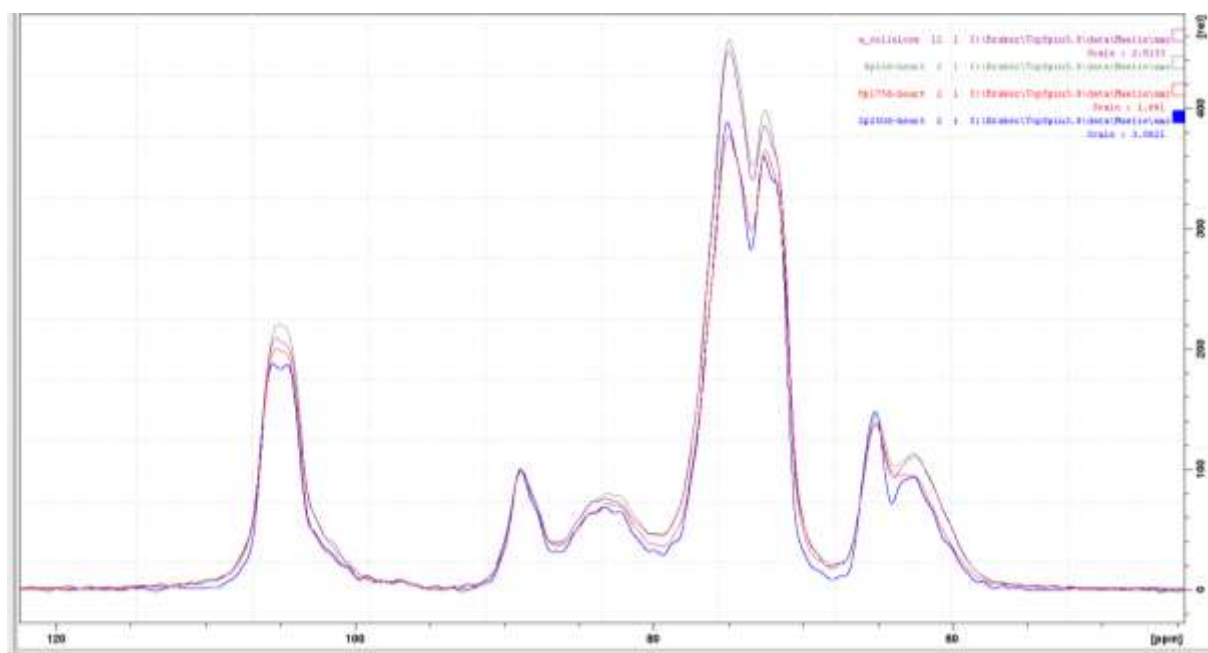


Fig. S-22: Spectra of compacted cellulose heart – full  $^{13}\text{C}$  CP-MAS NMR spectra – purple: untreated “ $\alpha$ -cellulose”, green: 8% $^{25^\circ\text{C}}$ , red: 8% $^{175^\circ\text{C}}$ , blue: 2% $^{250^\circ\text{C}}$

### Deconvolution of $^{13}\text{C}$ CP-MAS NMR spectra

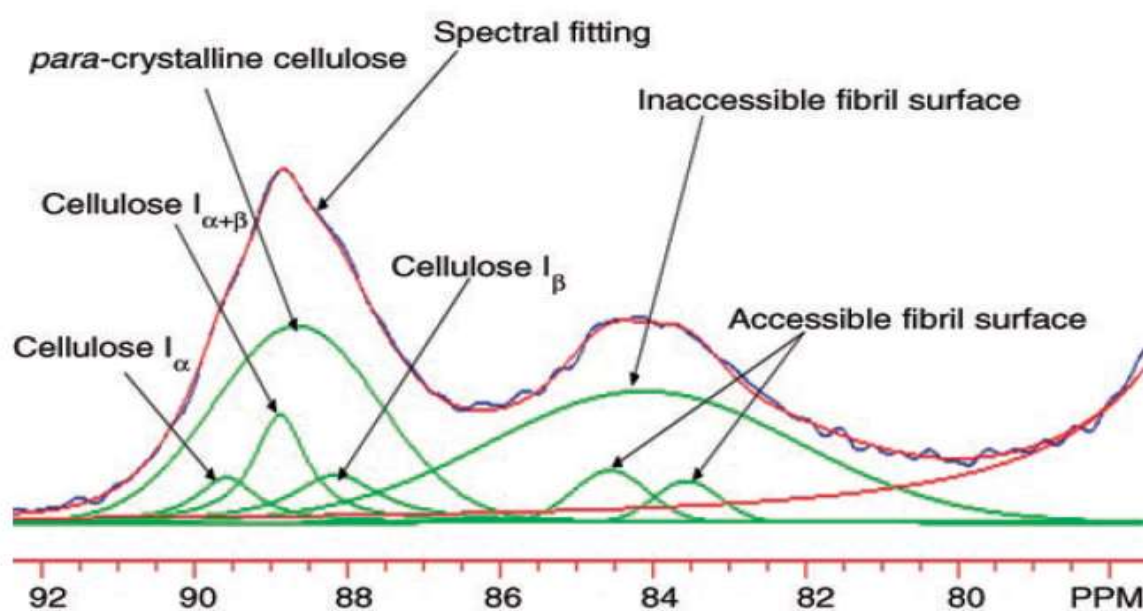


Fig. S-23: Spectral fitting for the C4 region of  $^{13}\text{C}$  CP-MAS NMR spectrum of native *Buddleja davidii* cellulose [6]

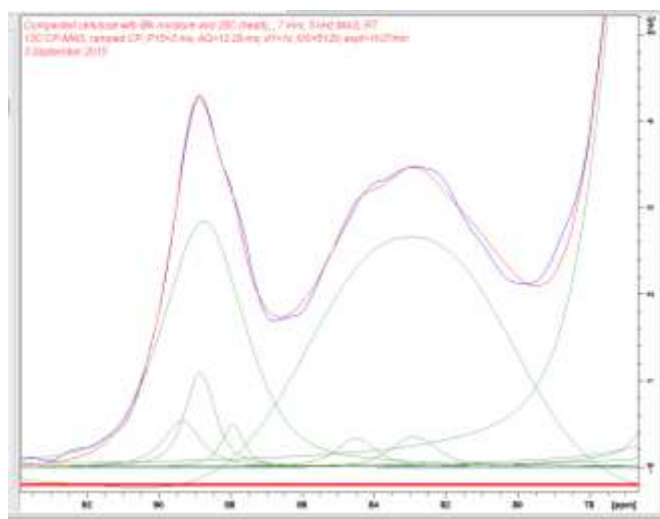


Fig. S-24: Spectral fitting for the C4 region of  $^{13}\text{C}$  CP-MAS NMR spectrum of compacted  $\alpha$ -cellulose 8%25°C faces

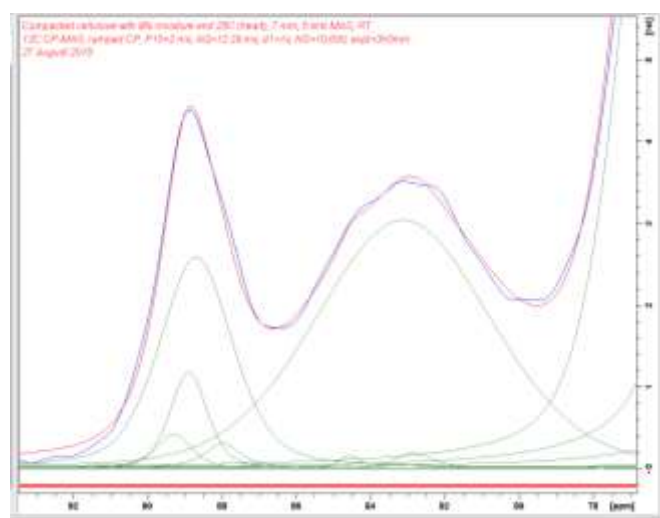


Fig. S-25: Spectral fitting for the C4 region of  $^{13}\text{C}$  CP-MAS NMR spectrum of compacted cellulose 8%25°C heart

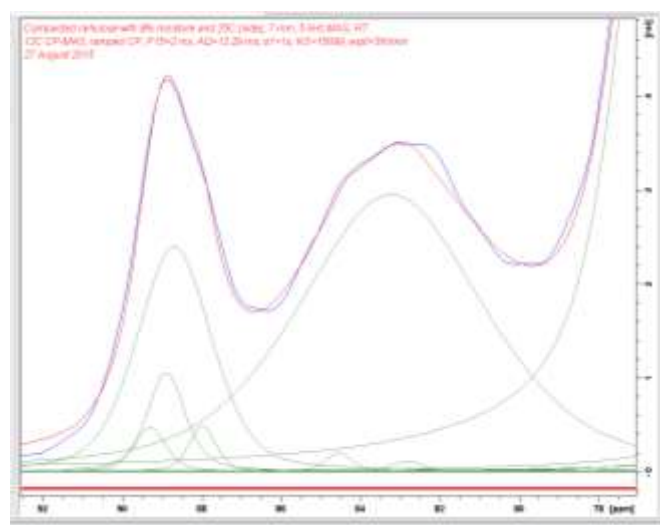


Fig. S-26: Spectral fitting for the C4 region of  $^{13}\text{C}$  CP-MAS NMR spectrum of compacted cellulose 8%25°C sides



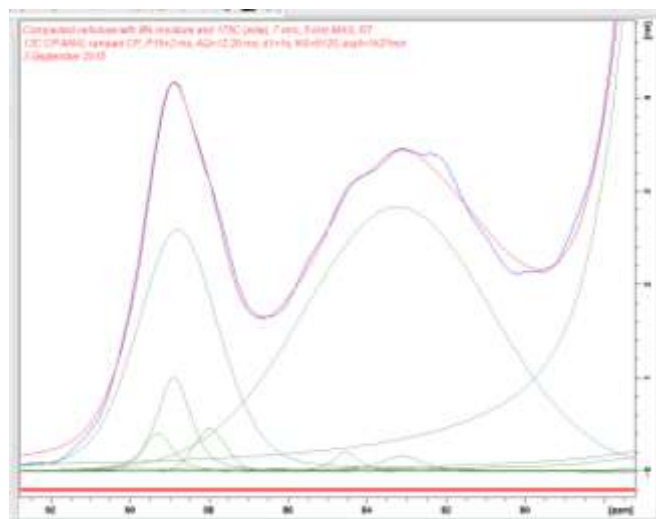


Fig. S-27: Spectral fitting for the C4 region of <sup>13</sup>C CP-MAS NMR spectrum of compacted cellulose 8%175°C sides

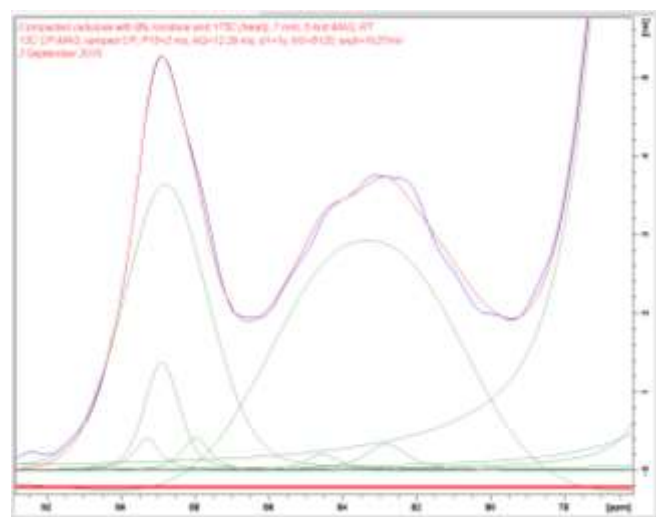


Fig. S-28: Spectral fitting for the C4 region of <sup>13</sup>C CP-MAS NMR spectrum of compacted cellulose 8%175°C heart

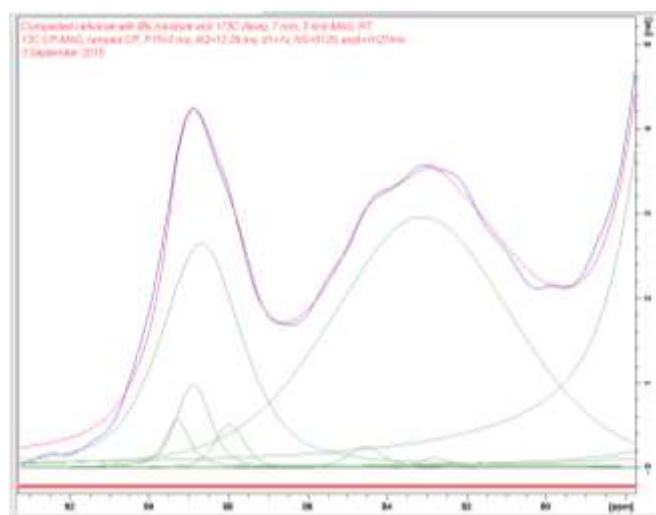


Fig. S-29: Spectral fitting for the C4 region of <sup>13</sup>C CP-MAS NMR spectrum of compacted cellulose 8%175°C faces

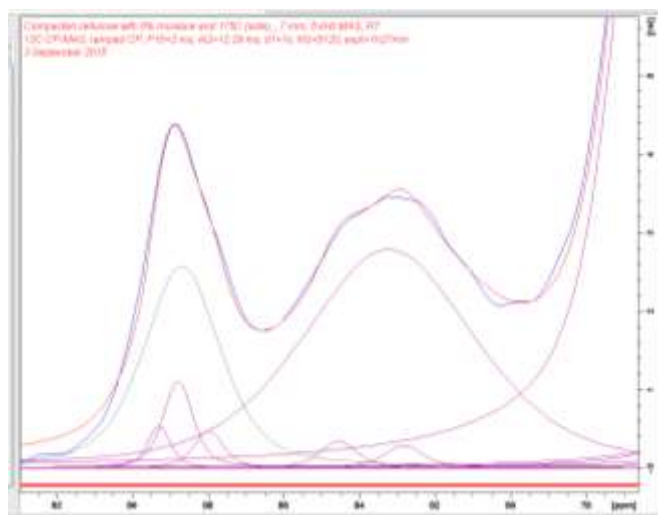


Fig. S-30: Spectral fitting for the C4 region of  $^{13}\text{C}$  CP-MAS NMR spectrum of compacted cellulose 0%175°C sides

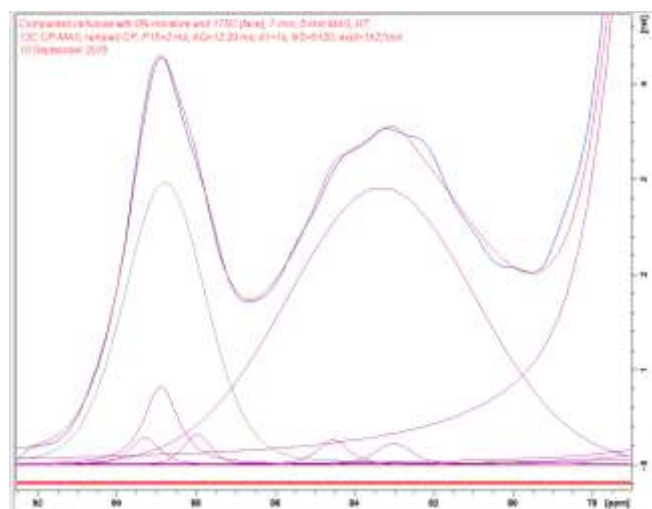


Fig. S-31: Spectral fitting for the C4 region of  $^{13}\text{C}$  CP-MAS NMR spectrum of compacted cellulose 0%175°C faces

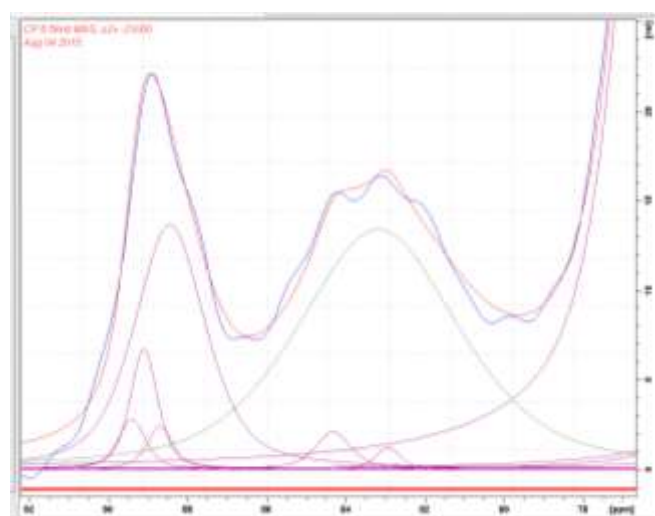


Fig. S-32: Spectral fitting for the C4 region of  $^{13}\text{C}$  CP-MAS NMR spectrum of compacted cellulose 2%250°C faces

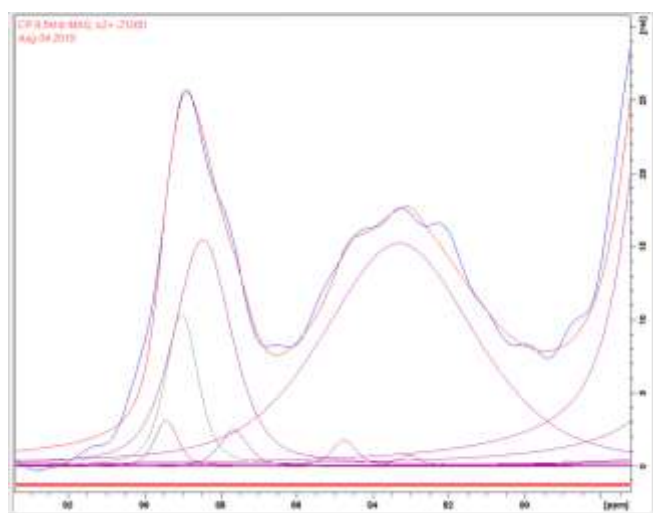


Fig. S-33: Spectral fitting for the C4 region of  $^{13}\text{C}$  CP-MAS NMR spectrum of compacted cellulose 2%250°C heart

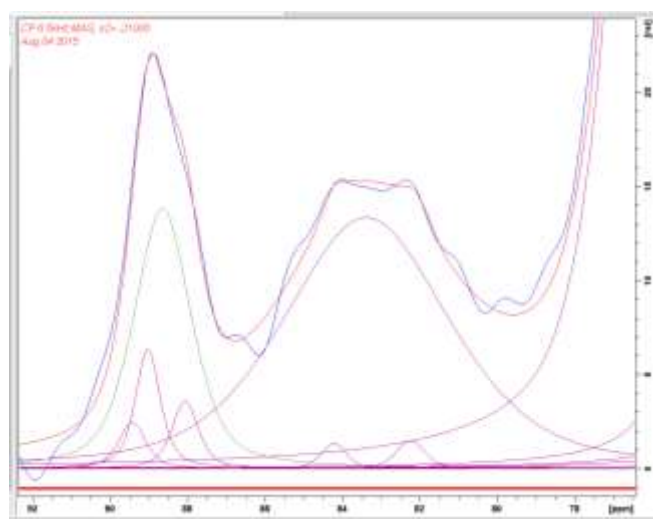


Fig. S-34: Spectral fitting for the C4 region of  $^{13}\text{C}$  CP-MAS NMR spectrum of compacted cellulose 2%250°C sides

## Comparison of XRD and solid-state NMR spectroscopy

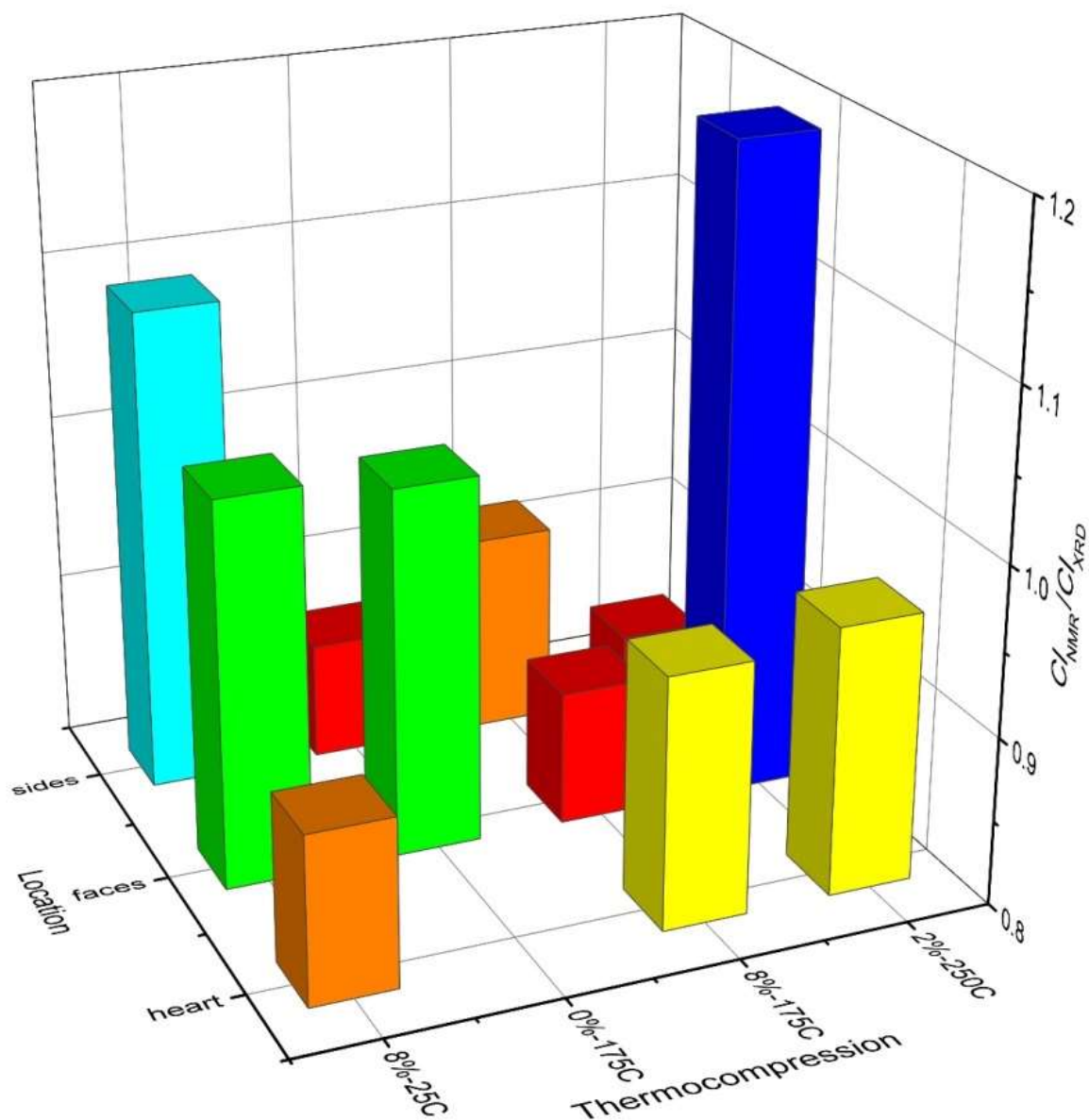


Fig. S-35: Comparison of crystallinity indices measured by XRD and solid-state NMR spectroscopy.

Cellulose has a complex hierarchical structure. Stating that there are only two types of domains, crystalline and amorphous domains, may be a misconception. There seems to be domains having short and medium range ordering in their lattice but lacking long-range ordering at least in one direction, the paracrystalline domains. Because of the existence of paracrystalline domains,  $CI$  depended on the measurement scale and thus on the method used for the measurement, XRD or spectroscopy (NMR and Raman). Solid-state NMR spectroscopy probes molecular features at shorter length scales than X-ray diffraction [7]. XRD and spectroscopy typically measure on the  $\mu\text{m}$  and  $\text{nm}$  range, respectively. This makes a difference, especially if paracrystalline domains are present (Fig. S-35). Paracrystalline domains are expected to be detected by spectroscopy as ordered (and typically be included in the parts of the sample described as crystalline), while they are not expected to be detected by XRD as ordered (and typically be included in the parts of the sample described as crystalline), see Fig. S-36.

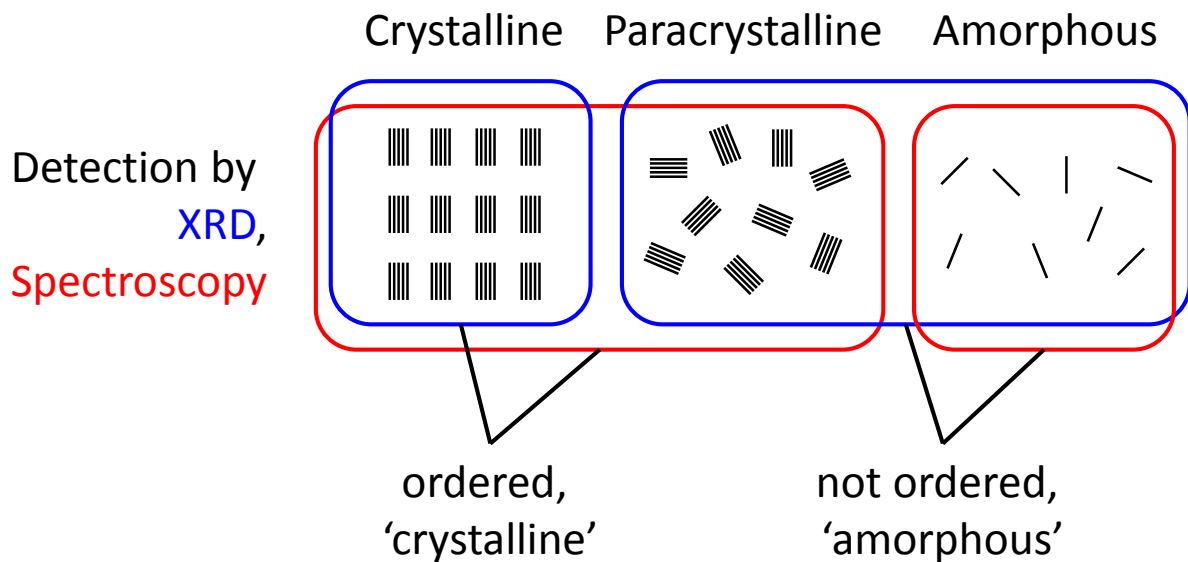


Fig. S-36: Difference in the detection of ordered domains by XRD and spectroscopy

## Mechanical Properties

	Temperature								
	175 °C		200 °C		225 °C		250 °C		
	Mean	SD	Mean	SD	Mean	SD	Mean	SD	
8	34.75	3.92	nd		30.24	5.38	37.02	2.04	Bending strength (MPa)
	35.65	2.84	33.93	4.27	40.23	2.98	44.48	1.46	
	35.21	2.59	34.92	5.02	41.73	1.79	44.84	3.15	
	43.17	6.29	45.3	7.78	55.09	4.7	70.1	4.14	
	35	1.79	41.13	2.03	39.62	3.38	51.73	5.74	
6	5.94	0.59	nd		6.23	0.44	7.11	0.33	Bending modulus (GPa)
	5.62	0.3	6.16	0.58	6.3	0.4	7.04	0.45	
	6.13	0.38	6.03	0.66	6.94	0.24	7.4	0.46	
	6.1	0.44	6.2	0.7	7.24	0.34	8.09	0.67	
	5.87	0.32	6.25	0.41	6.71	0.33	7.72	0.26	
4	17.19	1.24	nd		16.17	3.03	19.16	1	Tensile strength (MPa)
	22.3	1.85	15.29	8.77	25.09	3.2	27.55	1.92	
	18.39	2.47	20.37	1.87	20.59	1.55	22.8	3.93	
	19.15	1.7	23.35	1.45	24.27	3.13	31.13	5.91	
	18.14	1.28	16.45	3.42	20.62	1.11	25.22	1.33	
2	1.88	0.1	nd		1.96	0.03	1.99	0.07	Tensile Modulus (MPa)
	1.91	0.11	1.75	0.06	2.03	0.14	2.02	0.11	
	1.99	0.04	2	0.07	2.05	0.11	2.13	0.11	
	1.78	0.08	1.84	0.05	1.87	0.08	1.94	0.15	
	1.83	0.1	1.82	0.07	1.94	0.09	2	0.08	

Table S-3: Mechanical properties of compressed cellulose according to molding temperature and cellulose moisture content. The best mechanical properties obtained for 2 % MC are listed in bold. SD stands for standard deviation, nd stands for not determined.

## References

- [1] ASTM D1795:2013 (January 2013).
- [2] Schmitz S, Dona AC, Castignolles P, Gilbert RG, Gaborieau M (2009) Assessment of the extent of starch dissolution in dimethyl sulfoxide by <sup>1</sup>H NMR spectroscopy. *Macromol Biosci* 9:506-514.
- [3] Maniego AR, Sutton AT, Gaborieau M, Castignolles P (2017) Assessment of the branching quantification in poly(acrylic acid): is it as easy as it seems? *Macromolecules*, 50:9032-9041.
- [4] Schenzel K, Fisher S (2004) Application of FT Raman spectroscopy for the characterization of cellulose. *Lenzing Berichte* 83:64–70.
- [5] Agarwal UP, Reiner RS, Ralph SA (2010) Cellulose I crystallinity determination using FT–Raman spectroscopy: univariate and multivariate methods. *Cellulose* 17:721–733
- [6] Pu Y, Hallac B, Ragauskas AJ (2013) Plant biomass characterization: application of solution- and solid-state NMR spectroscopy, In: Wymann CE (ed) *Aqueous pretreatment of plant biomass for biological and chemical conversion to fuels and chemicals*, John Wiley & Sons, Chichester, chapter 18, pp 369-390. DOI: 10.1002/9780470975831.ch18
- [7] Gidley MJ, Robinson G (1990) Techniques for studying interactions between polysaccharides. In: *Methods in Plant Biochemistry*, Dey PM, Harborne JB (Eds), Academic Press, London, volume 2 Carbohydrates, chapter 18, pp 607-642.